NASA TN D-840

NASA TN D-840

TECHNICAL NOTE

D-840

AERODYNAMIC FORCE CHARACTERISTICS OF A SERIES OF LIFTING CONE AND CONE-CYLINDER CONFIGURATIONS AT A MACH NUMBER OF 6.83 AND ANGLES OF ATTACK UP TO 130°

By Jim A. Penland

Langley Research Center
Langley Field, Va.

NATIONAL AERONAUTICS AND SPACE ADMINISTRATION
WASHINGTON
June 1961

NATIONAL AERONAUTICS AND SPACE ADMINISTRATION

TECHNICAL NOTE D-840

AERODYNAMIC FORCE CHARACTERISTICS OF A SERIES OF LIFTING CONE AND CONE-CYLINDER CONFIGURATIONS AT A MACH NUMBER OF 6.83 AND ANGLES OF ATTACK UP TO 130°

By Jim A. Penland

SUMMARY

Force tests of a series of right circular cones having semivertex angles ranging from 5° to 45° and a series of right circular cone-cylinder configurations having semivertex angles ranging from 5° to 20° and an afterbody fineness ratio of 6 have been made in the Langley 11-inch hypersonic tunnel at a Mach number of 6.83, a Reynolds number of 0.24×10^6 per inch, and angles of attack up to 130°.

An analysis of the results made use of the Newtonian and modified Newtonian theories and the exact theory. A comparison of the experimental data of both cone and cone-cylinder configurations with theoretical calculations shows that the Newtonian concept gives excellent predictions of trends of the force characteristics and the locations with respect to angle of attack of the points of maximum lift, maximum drag, and maximum lift-drag ratio. Both the Newtonian and exact theories give excellent predictions of the sign and value of the initial lift-curve slope. The maximum lift coefficient for conical bodies is nearly constant at a value of 0.5 based on planform area for semivertex angles up to 30°. The maximum lift-drag ratio for conical bodies can be expected to be not greater than about 3.5, and this value might be expected only for slender cones having semivertex angles of less than 5°. The increments of angle of attack and lift coefficient between the maximum lift-drag ratio and the maximum lift coefficient for conical bodies decrease rapidly with increasing semivertex angles as predicted by the modified Newtonian theory.

INTRODUCTION

During the reentry of an orbital vehicle or missile into the atmosphere, the flight attitude may be modulated with time through large angles of attack for range control and for the alleviation of aerodynamic loading and heating. In addition, inadvertent maneuvers due to unprogramed or unforeseen perturbations, which may orient the vehicle in unusual positions, may occur. The results of any such behavior on structural loading and the possible alteration of the trajectory depend on the various forces imposed on the configuration at all possible flight attitudes. There is a need therefore for a systematic study of the aerodynamic characteristics of a wide range of possible shapes prior to the determination of possible extraterrestrial vehicles which make use of atmospheric braking for reentry.

Considerable data including force as well as pressure-distribution measurements have been compiled on sharp cone and cone-cylinder configurations at low angles of attack throughout the supersonic speed range. (See refs. 1 to 5.) The purpose of this investigation was to obtain force data on a series of cone and cone-cylinder configurations at angles of attack up to 130° at a Mach number of 6.83 and to compare the data with available theory. The analysis of the cone data was made with particular consideration of the regions in the vicinity of the maximum lift-drag ratio and the maximum lift coefficient, which are important parameters used in reentry trajectory calculations. (See refs. 6 to 9.) No consideration was given to aerodynamic heating; however, it may be expected that the necessary moderate blunting will alter the results and conclusions only slightly.

L1301

SYMBOLS

$C = \mu_w T_\infty / \mu_\infty T_w = 0.86$

C_A	axial-force coefficient, $\frac{F_A}{q_\infty S}$
C_D	drag coefficient, $\frac{F_D' - F_b \cos\alpha}{q_\infty S}$
C_F	average skin-friction coefficient, $\frac{1.328\sqrt{C}}{\sqrt{R}} \frac{2\sqrt{3}}{3} \frac{S_s}{S} \frac{q}{q_\infty}$
C_L	lift coefficient, $\frac{F_L - F_b \sin\alpha}{q_\infty S}$
ΔC_L	increment of lift coefficient between $(L/D)_{max}$ and $C_{L,max}$
C_{L_α}	lift-curve slope, $\frac{\partial C_L}{\partial \alpha}$
C_N	normal-force coefficient, $\frac{F_N}{q_\infty S}$

L1301

C_{N_α}	normal-force curve slope, $\frac{\partial C_N}{\partial \alpha}$
C_p	pressure coefficient, $\frac{p - p_\infty}{q_\infty}$
F_A	axial force along X-axis; positive direction, $-X$
F_b	base-pressure correction, $(p_\infty - p_b)S_b$
F_D'	$= F_N \sin \alpha + F_A \cos \alpha$
F_L	$= F_N \cos \alpha - F_A \sin \alpha$
F_N	normal force along Z-axis, positive direction, $-Z$
L/D	lift-drag ratio, C_L/C_D
M_∞	free-stream Mach number
p	local pressure
p_b	pressure on base of model
p_∞	free-stream static pressure
q	local dynamic pressure
q_∞	free-stream dynamic pressure
R	local Reynolds number
R_∞	free-stream Reynolds number based on body length
S	planform area of model
S_b	base area of model
S_s	total surface area excluding base area
T_w	wall temperature
T_∞	free-stream temperature
α	angle of attack, deg
$\Delta\alpha$	increment of angle of attack between $(L/D)_{max}$ and $C_{L,max}$

α_m	angle-of-attack location of maximum lift coefficient or maximum lift-drag ratio
θ_V	semivertex angle of cone
μ_w	wall dynamic viscosity
μ_∞	free-stream dynamic viscosity

Subscripts:

local	surface condition
max	maximum or stagnation
min	minimum

MODELS

The models used for the present tests may be seen in the photographs shown in figures 1 and 2 and in the detail drawings shown in figures 3 and 4. These models consisted of a series of six right circular cones having semivertex angles ranging from 5° to 45° and a series of four right circular cone-cylinder configurations having semivertex angles ranging from 5° to 20° and an afterbody fineness ratio of 6. All models were constructed of stainless steel and were attached directly to the strain-gage balance for angles of attack up to 25°. The models were attached to the balance by an auxiliary sting for the angle-of-attack range from 30° to 130° to make possible initial deflection settings on models with zero strut and balance settings.

APPARATUS AND TESTS

The tests were conducted in the Mach number 6.86 test section of the Langley 11-inch hypersonic tunnel. The boundary-layer thickness on the tunnel wall and hence the free-stream Mach number of this test section is dependent upon the stagnation pressure. For these tests, at an average stagnation pressure of 24 atmospheres and an average stagnation temperature of 675° F (to avoid liquefaction), the average free-stream Mach number was 6.83 and the average Reynolds number was 0.24×10^6 per inch. The absolute humidity was kept to less than 1.9×10^{-5} pounds of water per pound of dry air for all tests. Normal- and axial-force data were obtained by use of a two-component strain-gage force balance through an angle-of-attack range from 0° to approximately 130° at a sideslip angle of 0°. For the angles of attack up to 25° the model base pressures were measured, and the axial-force component was adjusted to correspond to a base pressure equal to the free-stream static pressure. Schlieren photographs were made at each angle-of-attack setting for all models, and the angle of attack was measured from the resulting negatives on an optical comparator.

ACCURACY OF DATA

L1301

The maximum uncertainties in the force coefficients for the individual test points due to the force-balance system are ±0.016 for the lift coefficient C_L and ±0.012 for the drag coefficient C_D. The stagnation pressure was measurable to an accuracy of ±0.06 atmosphere; the reading accuracy of the angle of attack was ±0.10°.

THEORETICAL METHODS

The aerodynamic force characteristics of the models at a Mach number of 6.83 throughout the angle-of-attack range of this investigation were calculated, and the results are presented along with the experimental data. The methods used for the various characteristics are discussed in this section.

Lift, Drag, and Lift-Drag Ratio

The values of C_L, C_D, and L/D were calculated by use of a modification of the Newtonian theory. This particular modification was used successfully to predict the loads on circular cylinders at high angles of attack in reference 10. The modification consists of the use of the Newtonian relation $C_{p,local} = C_{p,max} \sin^2\delta$ where δ is the deflection angle of the local flow and $C_{p,max}$ is the stagnation-pressure coefficient. A value of $C_{p,max}$ of 1.822 for $M_\infty = 6.83$ determined from normal-shock theory and verified by experiment (ref. 10) was used, instead of the value of $C_{p,max}$ of 2 determined from pure-momentum considerations (ref. 11). The integrated coefficients for both the cone and cone-cylinder configurations were determined by use of the basic Newtonian theory of reference 11 with the previously mentioned modification incorporated, unless otherwise specified.

An approximation of the average skin-friction coefficient was made by use of the following equation, which was obtained from reference 12 and modified for cones as suggested in reference 13:

$$C_F = \frac{1.328\sqrt{C}}{\sqrt{R}} \frac{2\sqrt{3}}{3} \frac{S_s}{S} \frac{q}{q_\infty}$$

For the tunnel conditions under consideration, a constant value of C of 0.86 was taken. The Reynolds number used was calculated for conditions on the surface of the cone at an angle of attack of 0°. The skin friction estimated by this method was assumed to be constant with varying angle of attack and was considered only in the discussion of maximum lift-drag ratio which occurs at relatively low angles of attack for cones with varying semivertex angles.

L
1
3
0
1

Lift-Curve Slope

The calculation of the lift-curve slope C_{L_α} of the right circular cones was made by use of the Newtonian impact theory (ref. 11) and the results of the exact theory (ref. 14).

Reference 11 states that the lift-curve slope for slender cones as determined by the impact theory is

$$(dC_L/d\alpha)_{\alpha=0^\circ} = (dC_N/d\alpha)_{\alpha=0^\circ} = \frac{d}{d\alpha}(\cos^2\theta_V \sin 2\alpha) = 2 \cos^2\theta_V$$

which reduces to the slender-body result of $dC_L/d\alpha = 2$ per radian at $\alpha = 0^\circ$, and this conclusion is valid for cones where $\theta_V \rightarrow 0$. However, for cones where θ_V is larger than 0° the value of C_{L_α} may be of different magnitude and/or sign. This result is due to the negative-lift contribution of axial force to the over-all lift of the cone which is readily seen in the equation for lift in terms of normal and axial forces as follows:

$$C_L = C_N \cos\alpha - C_A \sin\alpha \tag{1}$$

The axial force increases with increasing cone angle semivertex θ_V, and for cones of very large angles the value of $C_A \sin\alpha$ exceeds the value of $C_N \cos\alpha$ which results in a negative lift and hence a negative slope of the lift curve $-C_{L_\alpha}$.

The calculations of the lift-curve slope by Newtonian theory (ref. 11) were therefore made in the following manner:

$$C_N = \cos^2\theta_V \sin 2\alpha \tag{2}$$

$$C_A = 2 \sin^2\theta_V + \sin^2\alpha(1 - 3 \sin^2\theta_V) \tag{3}$$

L1301

Combining equations (1), (2), and (3) and simplifying gives

$$C_L = \cos^2\theta_V \sin 2\alpha \cos \alpha - 2 \sin^2\theta_V \sin \alpha - \sin^3\alpha + 3 \sin^3\alpha \sin^2\theta_V$$

Use of

$$\sin 2\alpha = 2 \sin \alpha \cos \alpha$$

and

$$\cos^2\alpha = 1 - \sin^2\alpha$$

results in

$$C_L = \sin^2\theta_V(-4 \sin \alpha + 5 \sin^3\alpha) + 2 \sin \alpha - 3 \sin^3\alpha \tag{4}$$

Differentiating with respect to α gives

$$\frac{dC_L}{d\alpha} = \sin^2\theta_V(-4 \cos \alpha + 15 \sin^2\alpha \cos \alpha) + 2 \cos \alpha - 9 \sin^2\alpha \cos \alpha$$

Use of

$$\sin^2\alpha = 1 - \cos^2\alpha$$

results in

$$\frac{dC_L}{d\alpha} = \cos \alpha\left[\sin^2\theta_V(11 - 15 \cos^2\alpha) - 7 + 9 \cos^2\alpha\right] \tag{5}$$

As equation (5) was derived by use of the results of reference 11, it is referenced on the cone base area and uses $C_{p,max}$ of 2. The use of $C_{p,max} = 2$ instead of $C_{p,max} = 1.822$ for this study of low angles of attack is discussed more fully in the section entitled "Results and Discussion." In this paper where the reference area is both the planform area and base area of the cone, the conversion factor is

$$\frac{\text{Base area}}{\text{Planform area}} = \pi \tan \theta_V$$

The calculation of C_{L_α} by use of the exact theory (ref. 14) makes use of the values of C_{N_α} and C_A for cones at an angle of attack of 0°. The assumption was made that these coefficients were unchanged for a change in angle of attack of 1°. These values of C_N and C_A were substituted into equation (1) along with the cosine and sine of 1° to obtain the values of C_{L_α} as used in this paper and referred to as the exact theory.

Maximum Lift

The maximum lift coefficient $C_{L,max}$ was determined by modified Newtonian theory where $C_{p,max} = 1.822$. For models where the $C_{L,max}$ occurred at angles of attack greater than the respective semivertex cone angle θ_V, the values of $C_{L,max}$ were obtained from faired curves calculated by the equations of reference 11 and modified for the normal-shock $C_{p,max}$ and for reference area. For those models where the $C_{L,max}$ occurred at angles of attack less than the respective semivertex cone angle, $C_{L,max}$ was obtained by setting equation (5) equal to zero and solving for α. This value of α was substituted into equation (4) to determine the value of $C_{L,max}$.

PRESENTATION OF RESULTS

The force coefficients are referred to the stability axis system. The presentation of the data on the right circular cones and the right circular cone-cylinder configurations is made separately. The basic longitudinal data on the cones is given first along with the results of calculations made by the modified Newtonian theory. These data are followed by analysis studies of the important details of the longitudinal force results of the cones and further comparisons with theoretical calculations. The basic longitudinal data on the cone-cylinder configurations is then presented along with the theoretical results and analysis figures. The scatter of the data above an angle of attack of 25° was due in part to the use of the auxiliary sting which supported the models. The figures presented are as follows:

L
1
3
0
1

Figure

Basic longitudinal force characteristics in pitch of cone models having semivertex angles of:
$\theta_V = 5^\circ$ 5
$\theta_V = 10^\circ$ 6
$\theta_V = 15^\circ$ 7
$\theta_V = 20^\circ$ 8
$\theta_V = 30^\circ$ 9
$\theta_V = 45^\circ$ 10

Schlieren photographs of right-circular-cone models 11

Variation of lift-curve slope with cone semivertex angle 12

Variation of maximum lift coefficient with cone semivertex angle 13

Variation of maximum lift-drag ratio with cone semivertex angle 14

Variation of the lift coefficient at $(L/D)_{max}$ and of the lift-drag ratio at $C_{L,max}$ with cone semivertex angle 15

Variation of the increments of angle of attack and lift coefficient between $(L/D)_{max}$ and $C_{L,max}$ with cone semivertex angle 16

Basic longitudinal force characteristics in pitch of cone-cylinder models having semivertex angles of:
$\theta_V = 5^\circ$ 17
$\theta_V = 10^\circ$ 18
$\theta_V = 15^\circ$ 19
$\theta_V = 20^\circ$ 20

Schlieren photographs of right circular cone-cylinder models 21

Variation of maximum lift-drag ratio with semivertex angle for cone-cylinder models 22

Correlation of various lifting bodies 23

RESULTS AND DISCUSSION

Lifting Cone Configurations

Basic cone data and theory.- A comparison of the basic experimental data and calculations made by use of the modified Newtonian theory (where $C_{p,max} = 1.822$) is made in figures 5 to 10 for the cones having semivertex angles ranging from 5° to 45°, respectively, with the planform area as the reference area. As the primary emphasis of this paper is on the high angle-of-attack range where the shocks are detached and a stagnation point or line is on the body, the modified Newtonian theory was used. The value of $C_{p,max}$ of 2 (ref. 11) should be used for the low angle-of-attack range so that closer approximations may be obtained, as may be seen subsequently in the discussion of the initial lift-curve slope. The results of the comparison between the calculations based on the modified Newtonian or impact concept with experimental data show nothing unusual. As expected, the theory gives excellent predictions of trends of the force characteristics, the location with respect to the angle of attack of the points of maximum lift, maximum drag, and maximum lift-drag ratio, and predictions of the exact values of the coefficients with sufficient accuracy for use in determining the over-all characteristics of the cone. Generally, the variation between the experimental data and theoretical estimates increases with cone semivertex angle. At low angles of attack the lift-drag ratio of the sharper cones, where the effects of skin friction are appreciable compared to the effects of pressure forces, is overpredicted by the theory. For the over-all range of cone semivertex angles and the range of angles of attack tested, both the trends in the variation of the lift coefficient with angle of attack and the values of the individual points are more consistently predicted than are the trends and values of the drag coefficient.

Schlieren photographs of all cone models are presented in figure 11 for a range of angles of attack from 0° to 90°. The method of model support is apparent in this figure for angles of attack above 30°.

Reference area.- Although the planform area was used for reference in the presentation of the basic data, other reference areas were considered during the analysis. These references were primarily the base area of the model and the volume of the model to the power of 2/3. When these reference areas are equated to the planform area, the conversion is found to be a function of semivertex angle θ_V as shown in the following equations:

$$\frac{\text{Planform area}}{\text{Base area}} = \frac{1}{\pi \tan \theta_V}$$

$$\frac{\text{Planform area}}{\text{Volume}^{2/3}} = \frac{3^{2/3}}{\pi^{2/3}\tan^{1/3}\theta_V}$$

These equations may be used to convert the plotted experimental or theoretical values to a new reference area. It should be noted, however, that the conversion ratios for both reference areas (that is, the ratio of the planform area to the base area and the ratio of the planform area to the volume to the power of 2/3) have tangent θ_V functions in the denominator; therefore, the results shown by a plot having θ_V as the variable will approach either 0 or ∞ as $\theta_V \rightarrow 0^\circ$ depending on the parameter. In order to be consistent the planform area was used on all analysis plots, and the use of the base area and the volume to the power of 2/3 as references was discussed where applicable.

Cone lift-curve slope.- The variation of the initial lift-curve slope is shown in figure 12 for cones of various semivertex angles. The data are shown for both base-area and planform-area reference and are compared with the slopes calculated by use of the Newtonian theory and a variation of the exact theory as discussed in the section entitled "Theoretical Methods." The lift-curve slope is important in the determination of equilibrium flight conditions for a lifting-body-type vehicle, to establish the attitude of flight, and in the determination of the over-all performance. The dynamic stability of either a ballistic or lifting vehicle is affected greatly by this stability derivative as it is an important contribution to the damping of the longitudinal short-period mode, especially for short-coupled vehicles.

Figure 12 shows that reasonable values of the slope C_{L_α} may be obtained by use of either the Newtonian or exact theories and that the two theories give nearly the same results for a change in angle of attack of 1°. The agreement between the experimental data and the theoretical estimates is reasonably good considering that at these low angles of attack the experimental forces were low and that the slopes were obtained from faired curves. Both theory and experiment show that as the cones become blunter (higher semivertex angles) the lift-curve slope decreases and becomes zero for cones having semivertex angles of 45°. For higher semivertex angles than 45° the lift-curve slope becomes negative; thus, the dynamic stability characteristics of any cone-shaped vehicle would be adversely affected. This effect further indicates that the lift contribution may be negative if the configuration is sufficiently blunt. The data point shown in figure 12 at $\theta_V = 90^\circ$ represents a flat disk from reference 15. The use of the planform area for reference is usually made for lifting-type bodies or vehicles. In this connection it may be seen that there is an optimum cone semivertex angle for the development of the lift-curve slope. A conical lifting body having a semivertex cone angle of about 26° would produce the most positive lift per degree of angle of attack. The curves of the lift-curve slope based on planform area and base area cross at a semivertex angle of 17.68°. A cone with this semivertex angle has a planform area equal to the base area. Equating the equation for planform area to the equation for base area and solving for the semivertex angle θ shows that the two areas are equal for a cone where $\theta_V = \tan^{-1} 1/\pi = 17.68^\circ$. The results when the volume to the power of 2/3 is used as reference are quite similar to the results when the planform area is used as reference except that the maximum C_{L_α} occurs at $\theta_V = 22^\circ$.

Maximum lift.- The variation of the maximum equilibrium lift coefficient and the angle of attack at which it occurs with cone semivertex angle is presented on figure 13. As the maximum lift coefficient determines the minimum speed for a given altitude that a vehicle can sustain level flight as well as being a factor in the longitudinal dynamics of a configuration and a parameter used in reentry trajectory calculations, it is important that it be given particular consideration. A study of the experimental and calculated results given in figure 13 shows that there is a gradual increase in the maximum lift coefficient with increasing cone semivertex angle up to a maximum which occurs at a semivertex angle of approximately 25°. For semivertex angles greater than 25°, a rapid decrease in $C_{L,max}$ occurs with increasing θ_V until $C_{L,max} = 0$ for a cone having $\theta_V = 45^\circ$. The experimental values for $\theta_V = 0^\circ$ plotted in this figure and other figures in this paper are for a circular cylinder. (See ref. 10.) The angle of attack at which the maximum lift occurs decreases from an angle of 55° for a cone having $\theta_V = 0^\circ$, or a circular cylinder, to $\alpha_m = 0^\circ$ for the blunt cone having $\theta_V = 45^\circ$. It appears that both the maximum lift coefficient and the angle of attack at which it occurs are both predicted with reasonable accuracy by the Newtonian concept. As is well known, the exact theory predicts that the shock detaches from cones having a semivertex angle of approximately 56° and above at an angle of attack of 0° for $M_\infty = 6.83$. From figure 13 it may be observed that when a cone is at an angle of attack such that its windward surface is oriented at about 56° to the flow, the maximum lift occurs. This phenomenon is denoted in figure 13 by a plot of the equation $\theta_V + \alpha_m = 56^\circ$ which for all semivertex angles below approximately 40° gives about as good an estimate of the angle of attack where $C_{L,max}$ occurs as does the Newtonian theory.

A careful examination of the schlieren photographs (fig. 11) through the range of angles of attack near $C_{L,max}$ shows that the shock profile adjacent to the body surface changed from straight to curved with increasing angle of attack. This curvature of shock profile was in addition to that downstream of the base of the body due to the expansion of the flow around the base of the model. The change was not abrupt but rather gradual over the angle-of-attack region where $C_{L,max}$ occurred.

Maximum lift-drag ratio.- The variation of the maximum lift-drag ratio and the angle of attack at which it occurs with cone semivertex angle are presented in figure 14. The maximum lift-drag ratio of a lifting reentry body is important in the determination of the maximum range, maximum deceleration, aerodynamic heating, loading, and control during reentry trajectory calculations. For a given vehicle the maximum range and minimum-peak deceleration occur when reentry takes place at $(L/D)_{max}$. For low heating rates both a high L/D and C_L are desirable. If a low total-heat input is required and a high deceleration is acceptable, reentry at low values of L/D and C_L is desirable.

Calculations of $(L/D)_{max}$ are presented with and without estimated skin friction and were made as described in the section entitled "Theoretical Methods." Without the addition of skin friction, the same results are obtained with either Newtonian or modified Newtonian theory. Figure 14 shows that the $(L/D)_{max}$ decreases and the angle of attack at which $(L/D)_{max}$ occurs increases with increasing cone semivertex angle. Similar effects are experienced by a body when the bluntness and hence drag is increased. The addition of skin friction to the Newtonian calculations of L/D improved the over-all theoretical estimates particularly for the cones having small semivertex angles. No curve was included for the angle of attack where $(L/D)_{max}$ occurs for the case with skin friction although calculations show that the angle of attack would increase only about 1° for any given semivertex angle. The modified Newtonian calculation of $(L/D)_{max}$ with skin friction more nearly predicts the wind-tunnel results than does the Newtonian calculation with skin friction. At the low angles of attack where $(L/D)_{max}$ occurred for all bodies tested, the Newtonian calculation should have given the closer approximation. This difference between the Newtonian and experimental results gives an idea as to the magnitude of the possible error in the skin-friction estimate. From this study of the experimental and calculated maximum lift-drag ratios for sharp cones of various semivertex angles, it appears that the maximum lift-drag ratio that may be expected is not greater than about 3.5 for low Reynolds number laminar-flow conditions and this value may be expected only for slender cones having semivertex angles of less than 5°. The semivertex angles for maximum lift-drag ratios of 2, 1, and 1/2 are about 8°, 16.5°, and 26°, respectively.

Lift at maximum lift-drag ratio.- The variation of the lift coefficient at the point of maximum lift-drag ratio is given in figure 15 for cones having various semivertex angles. The lift coefficient at $(L/D)_{max}$ increases with increasing cone semivertex angle and reaches a maximum of almost 0.5 for a 28° semivertex angle cone, and decreases rapidly thereafter to zero for a 45° semivertex angle cone. The use of either the base area of the volume to the power of 2/3 as reference area gave similar trends to those shown in figure 15 where the planform area was used; however, the calculated curves attained maximum values at lower cone semivertex angles of approximately 21° and 26° for base area and volume to the power of 2/3, respectively.

Lift-drag ratio at $C_{L,max}$.- Also presented on figure 15 are the values of L/D taken at the point of $C_{L,max}$ for various semivertex angles. The values of L/D remain relatively constant for cone semivertex angles up to approximately 20° and then decrease gradually to zero for a 45° semivertex angle.

L
1
3
0
1

Increments of α and C_L between $(L/D)_{max}$ and $C_{L,max}$.- The calculated and measured values of the increments of angle of attack and lift coefficient between the values of maximum lift-drag ratio and maximum lift coefficient are presented in figure 16, and both decrease rapidly with increasing semivertex angle. As noted in the discussion of maximum lift-drag ratio presented in figure 14, the $(L/D)_{max}$ decreases with increasing θ_V; therefore, both the increments of α and C_L between $(L/D)_{max}$ and $C_{L,max}$ also decrease with decreasing $(L/D)_{max}$. The calculated results by use of the modified Newtonian theory give excellent predictions of these increments for the conical bodies tested.

Determination of optimum conical lifting-body vehicles.- The foregoing study of a series of conical bodies having semivertex angles up to 45° makes it possible to make a first approximation as to what configuration might be optimum based on the parameters C_L and L/D which are two of the more important force characteristics for reentry trajectory calculations. The maximum lift-curve slope occurs for a cone having a 26° semivertex angle. The maximum lift coefficient occurs for a cone having a 24° semivertex angle. The product of the value of C_L at $(L/D)_{max}$ and the value of L/D at $C_{L,max}$ reaches a maximum for a cone having a 23° semivertex angle. This result indicates that the cone having a 23° semivertex angle is the best compromise in the region between $(L/D)_{max}$ and $C_{L,max}$. Such a conical body could be expected to have a maximum lift-drag ratio of approximately 0.6 and $\Delta\alpha$ and ΔC_L between $(L/D)_{max}$ and $C_{L,max}$ of approximately 11° and 0.09, respectively, and would have a positive lift-curve slope. The final optimum body shape would have to be selected on the basis of allowable weight, size, and aerodynamic heating, which are criteria beyond the scope of the present paper.

Lifting Cone-Cylinder Configurations

Basic cone-cylinder data and theory.- A comparison of the basic experimental longitudinal force characteristics and calculations made through the use of the modified Newtonian theory (where $C_{p,max} = 1.822$) is shown in figures 17 to 20 for right circular cone-cylinder configurations having semivertex angles of 5° to 20° and an afterbody fineness ratio of 6. For these data, the planform area was used as reference. For those who wish to use the base area as reference the following ratios of planform area to base area are given:

L
1
3
0
1

θ_V, deg	S/S_b
5	11.279
10	9.443
15	8.827
20	8.514

A study of these data shows that the modified Newtonian theory gives excellent predictions of the trends of the lift and drag forces with varying angle of attack and the points within the angle-of-attack range where the maximum lift, maximum drag, and maximum lift-drag ratio occur. In general, the accuracy with which the predicted forces may be made on the cone-cylinder configurations studied herein is superior to that made by the same method on the simple cone configurations. This result can be explained by the fact that the cylindrical portion of the cone-cylinder configurations makes up the larger portion of the configuration and that the basic Newtonian or impact concept assumes that the shock lies close to the surface as may be seen in the schlieren photographs in figure 21 for the detached-flow conditions around the windward or high-pressure side of the cylindrical afterbody. As no skin friction was taken into account, the results of the lift-drag-ratio calculation are much more in error for the configurations with the higher fineness ratios, but greatly improve with increasing cone semivertex angle where the over-all effects of the viscous forces are reduced. As expected from the study of the conical-body series, the angle of attack for maximum lift-drag ratio increased with the increased drag of the blunter cones, and the point at which the maximum lift occurred remained nearly fixed. A summary of the maximum lift-drag ratios and the angle of attack at which they occur is presented in figure 22 for the series of cone-cylinder configurations tested.

Correlation of Lifting Bodies

A correlation of both the cone and the cone-cylinder configurations of the present paper is shown in figure 23, which makes use of the relations $C_{L,max}/C_{D,min}$ and $(L/D)_{max}$ as used and discussed in references 16 and 7. This type of plot was used in reference 16 to correlate a large variety of lifting bodies, and the importance of the ratios $C_{L,max}/C_{D,min}$ and $(L/D)_{max}$ in the minimization of satellite reentry acceleration was discussed in reference 7. In addition to the data of this investigation, several points taken from the data of the spherically blunted right circular cones of reference 16 which had nose bluntnesses equal to 0.2 of the base diameter are plotted in figure 23. When the lift and drag data for the several models are plotted as shown in figure 23, a relatively smooth curve, which is predicted with reasonable accuracy by the Newtonian theory, results.

Figure 23 shows the possibility that if experimental studies of a body are made up to an angle of attack high enough to obtain $(L/D)_{max}$ the value of $C_{L,max}$ could be approximated from the curve of this figure; thus, the determination of force characteristics can be made.

CONCLUSIONS

Analysis of experimental data obtained from tests at a Mach number of 6.83 and a Reynolds number of 0.24×10^6 per inch made in the Langley 11-inch hypersonic tunnel on right circular cones and right circular cone-cylinder configurations having an afterbody fineness ratio of 6 leads to the following conclusions:

1. The Newtonian or impact theory gives excellent predictions of trends of the force characteristics of all configurations tested and the locations with respect to the angle of attack of the points of maximum lift, maximum drag, and maximum lift-drag ratio. Generally, the calculations by the Newtonian concept predict the experimental results with greater accuracy for those configurations having the higher fineness ratios, particularly, for those configurations where the windward shock lies close to the body surface.

2. For a change of 1° in angle of attack of conical bodies, either the Newtonian or exact theory gives excellent predictions of the sign and magnitude of the initial lift-curve slope. Both the theoretical predictions and the experimental data give values of the lift-curve slope that are negative for cones having semivertex angles of 45° and greater.

3. For those cones having semivertex angles between 0° and 90°, a cone having a semivertex angle of approximately 26° exhibits the highest positive value of initial lift-curve slope.

4. A gradual change in the shock-profile shape adjacent to the body surface from straight to curved takes place over the angle-of-attack range near the maximum lift coefficient. The maximum lift coefficient is essentially constant at a value of approximately 0.5 based on plan-form area for cones having semivertex angles up to approximately 30°. The angle of attack at which the maximum lift occurs is predicted reasonably well by either the Newtonian theory or by the empirical relation which states that the sum of the angle of attack at which the maximum lift occurs and the cone semivertex angle is equal to 56°.

5. The maximum lift-drag ratio that may be expected for a cone is not greater than about 3.5 and this value might be expected for slender cones having semivertex angles of less than 5°. The semivertex angles for maximum lift-drag ratios of 2, 1, and 1/2 are about 8°, 16.5°, and 26°, respectively.

6. The increments of angle of attack and lift coefficient between the maximum lift-drag ratio and the maximum lift coefficient for conical bodies decrease rapidly with increasing semivertex angle and decreasing maximum lift-drag ratio and are well predicted by the modified Newtonian theory.

7. Based on the values of the lift coefficient and the lift-drag ratio, the optimum conical lifting body within the limiting semivertex-angle range of 0° to 45° has a semivertex angle of 23° and could be expected to have a maximum lift-drag ratio of approximately 0.6 and increments of angle of attack and lift coefficient between the maximum lift-drag ratio and the maximum lift coefficient of approximately 11° and 0.09, respectively, and would have a positive lift-curve slope.

Langley Research Center,
National Aeronautics and Space Administration,
Langley Field, Va., March 17, 1961.

REFERENCES

1. Cooper, Ralph D., and Robinson, Raymond A.: An Investigation of the Aerodynamic Characteristics of a Series of Cone-Cylinder Configurations at a Mach Number of 6.86. NACA RM L51J09, 1951.

2. Ridyard, Herbert W.: The Aerodynamic Characteristics of Two Series of Lifting Bodies at Mach Number 6.86. NACA RM L54C15, 1954.

3. Oliver, Robert E.: An Experimental Investigation of Flow Over Simple Blunt Bodies at a Nominal Mach Number of 5.8. GALCIT Memo. No. 26, (Contract No. DA-04-495-Ord-19), June 1, 1955.

4. Liccini, L. L.: Hypersonic Tunnel No. 4 Results IX: The Development of a Water-Cooled Strain-Gage Balance (Including Sting Effects) and Its Application to a Study of Normal Force and Pitching Moments of a Cone and Cone-Cylinder at Mach Numbers 5 to 8. NAVORD Rep. 4334, U.S. Naval Ord. Lab. (White Oak, Md.), Aug. 20, 1956.

5. Lehnert, R., and Schermerhorn, V. L.: Wake Investigation on Sharp and Blunt Nose Cones at Supersonic Speeds. NAVORD Rep. 5668, U.S. Naval Ord. Lab. (White Oak, Md.), Jan. 28, 1958.

6. Lees, Lester, Hartwig, Frederic W., and Cohen, Clarence B.: Use of Aerodynamic Lift During Entry Into the Earth's Atmosphere. ARS Jour., vol. 29, no. 9, Sept. 1959, pp. 633-641.

7. Grant, Frederick C.: Importance of the Variation of Drag With Lift in Minimization of Satellite Entry Acceleration. NASA TN D-120, 1959.

8. Grant, Frederick C.: Analysis of Low-Acceleration Lifting Entry From Escape Speed. NASA TN D-249, 1960.

9. Becker, John V.: Heating Penalty Associated With Modulated Entry Into Earth's Atmosphere. ARS Jour. (Tech. Notes), vol. 30, no. 5, May 1960, pp. 504-505.

10. Penland, Jim A.: Aerodynamic Characteristics of a Circular Cylinder at Mach Number 6.86 and Angles of Attack up to 90°. NACA TN 3861, 1957. (Supersedes NACA RM L54A14.)

11. Grimminger, G., Williams, E. P., and Young, G. B. W.: Lift on Inclined Bodies of Revolution in Hypersonic Flow. Jour. Aero. Sci., vol. 17, no. 11, Nov. 1950, pp. 675-690.

12. Chapman, Dean R., and Rubesin, Morris W.: Temperature and Velocity Profiles in the Compressible Laminar Boundary Layer With Arbitrary Distribution of Surface Temperature. Jour. Aero. Sci., vol. 16, no. 9, Sept. 1949, pp. 547-565.

13. Eckert, Ernst R. G.: Survey on Heat Transfer at High Speeds. WADC Tech. Rep. 54-70, U.S. Air Force, Apr. 1954.

14. Ames Research Staff: Equations, Tables, and Charts for Compressible Flow. NACA Rep. 1135, 1953. (Supersedes NACA TN 1428.)

15. Penland, Jim A., and Armstrong, William O.: Static Longitudinal Aerodynamic Characteristics of Several Wing and Blunt-Body Shapes Applicable for Use as Reentry Configurations at a Mach Number of 6.8 and Angles of Attack up to 90°. NASA TM X-65, 1959.

16. Armstrong, William O.: Hypersonic Aerodynamic Characteristics of Several Series of Lifting Bodies Applicable to Reentry Vehicle Design. NASA TM X-536, 1961.

L
1
3
0
1

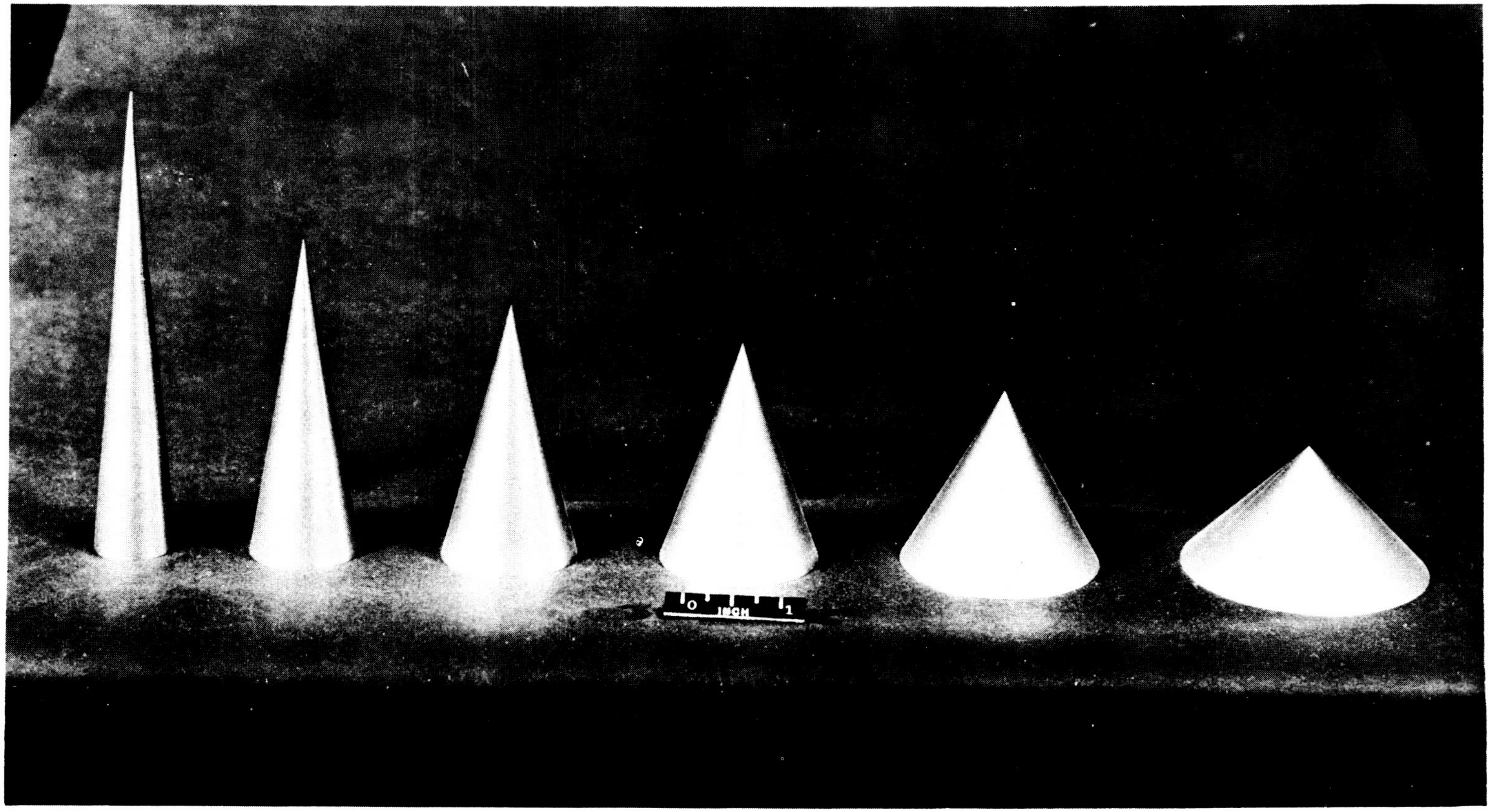

Figure 1.- Photograph of cone models. L-59-8492

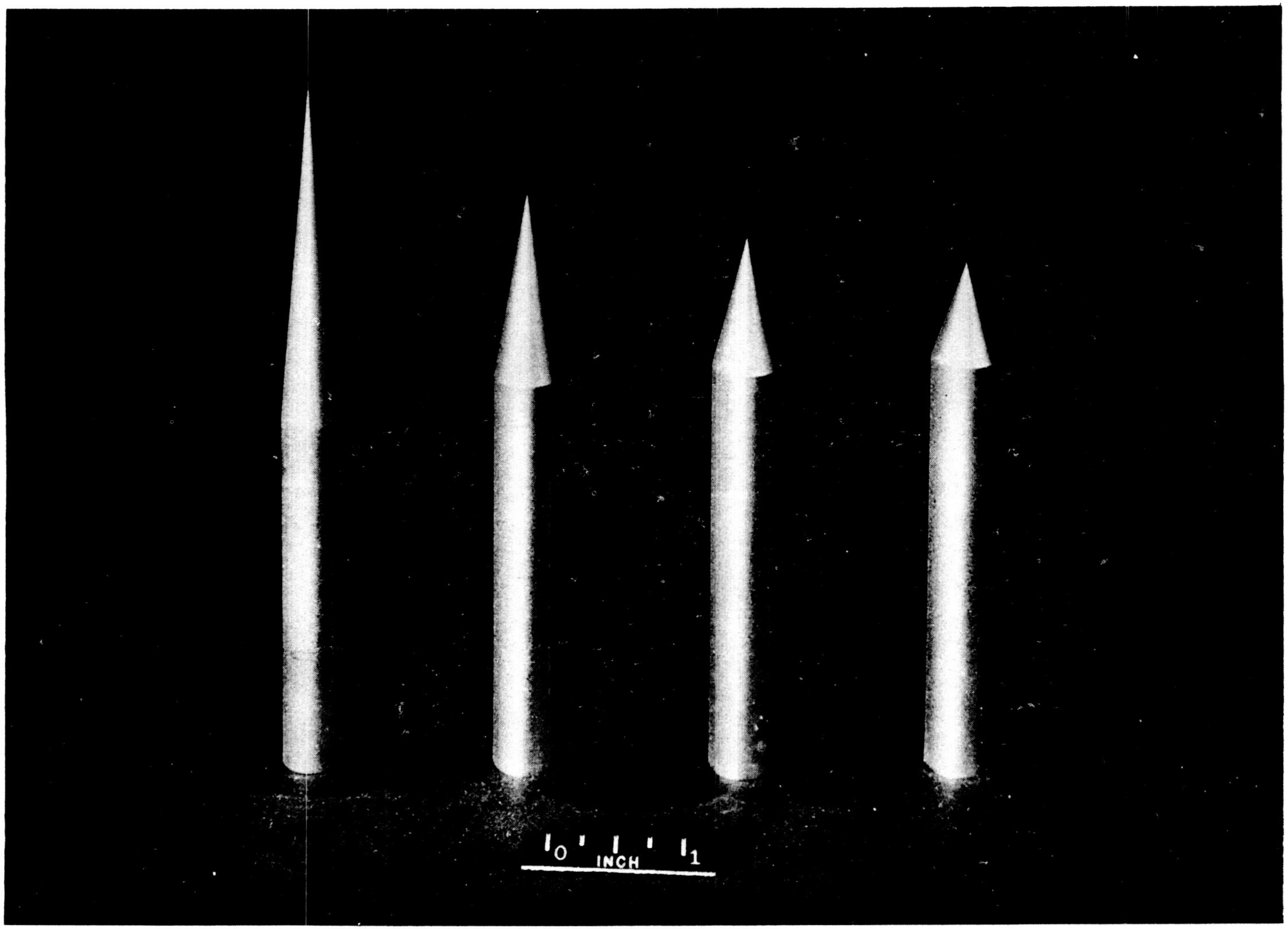

L-59-8493

Figure 2.- Photograph of cone-cylinder models having an afterbody fineness ratio of 6.

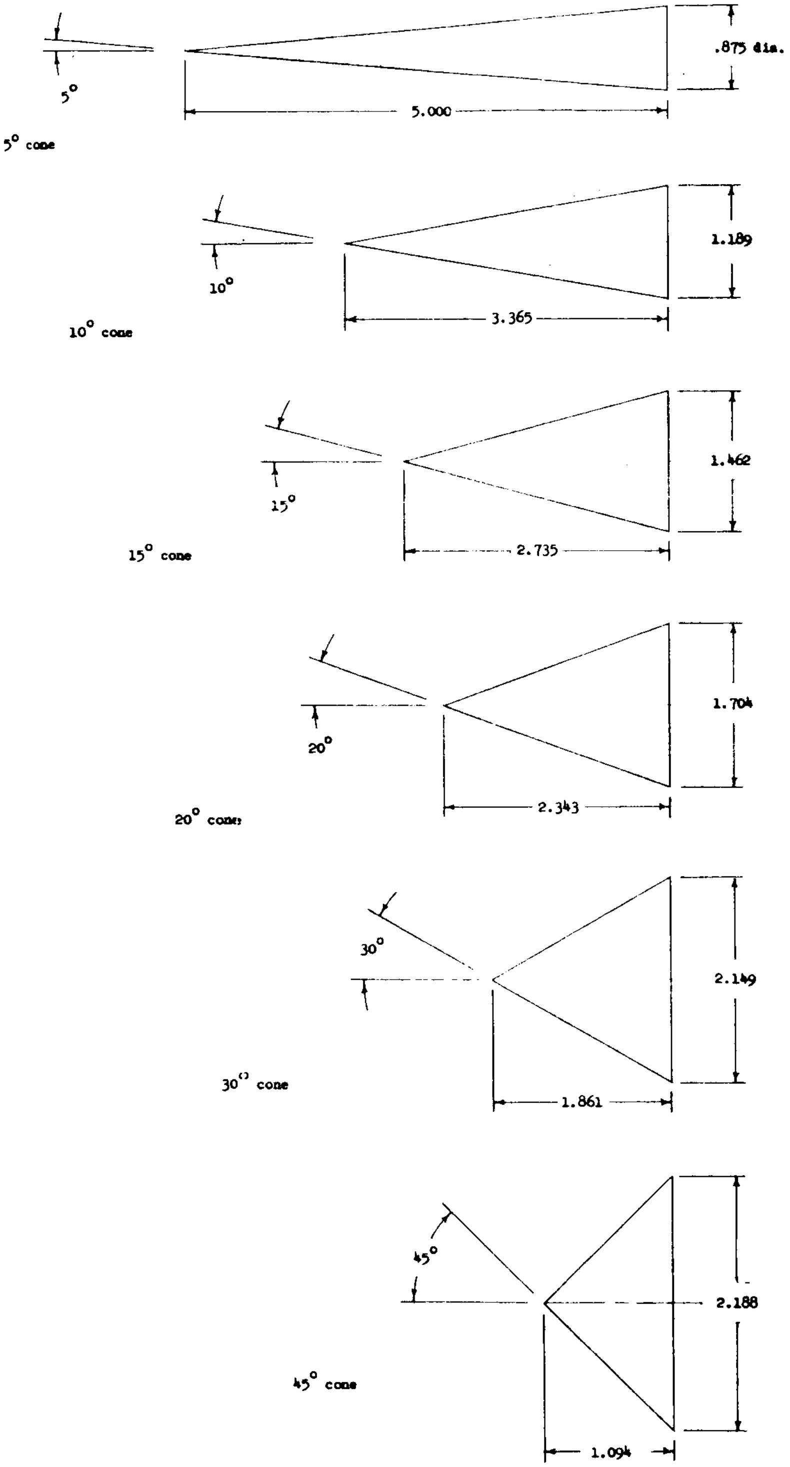
5°
.875 dia.
5.000
5° cone
10°
1.189
3.365
10° cone
15°
1.462
2.735
15° cone
20°
1.704
2.343
20° cone
30°
2.149
1.861
30° cone
45°
2.188
1.094
45° cone

L-1301

Figure 3.- Details of cone models. Dimensions are in inches.

L-1301

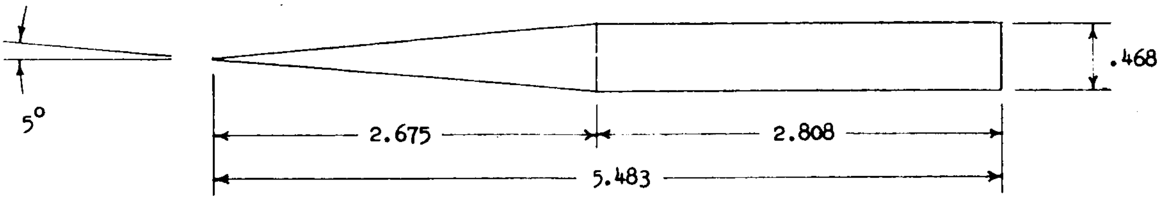
5°
2.675
2.808
5.483
.468

5° cone-cylinder

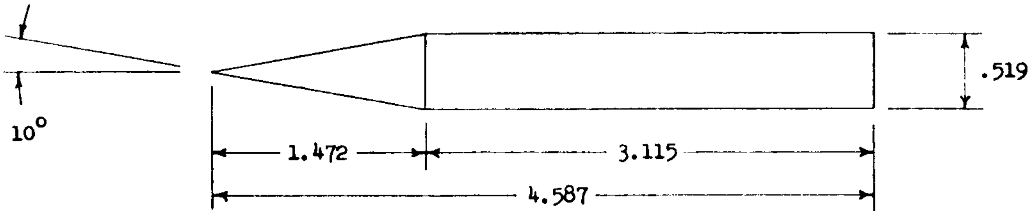
10°
1.472
3.115
4.587
.519

10° cone-cylinder

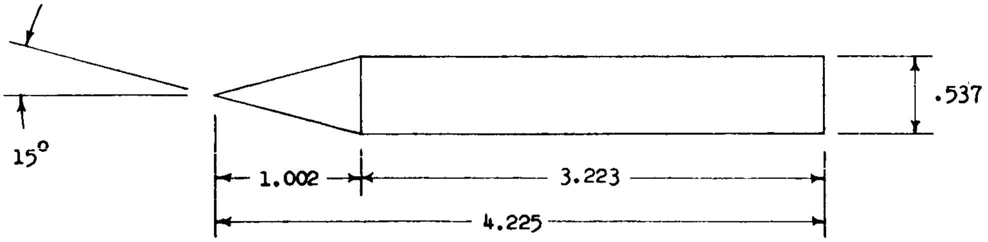
15°
1.002
3.223
4.225
.537

15° cone-cylinder

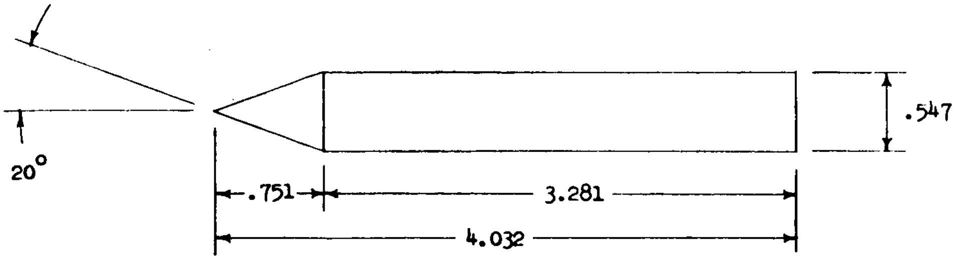
20°
.751
3.281
4.032
.547

20° cone-cylinder

Figure 4.- Details of cone-cylinder models. Dimensions are in inches.

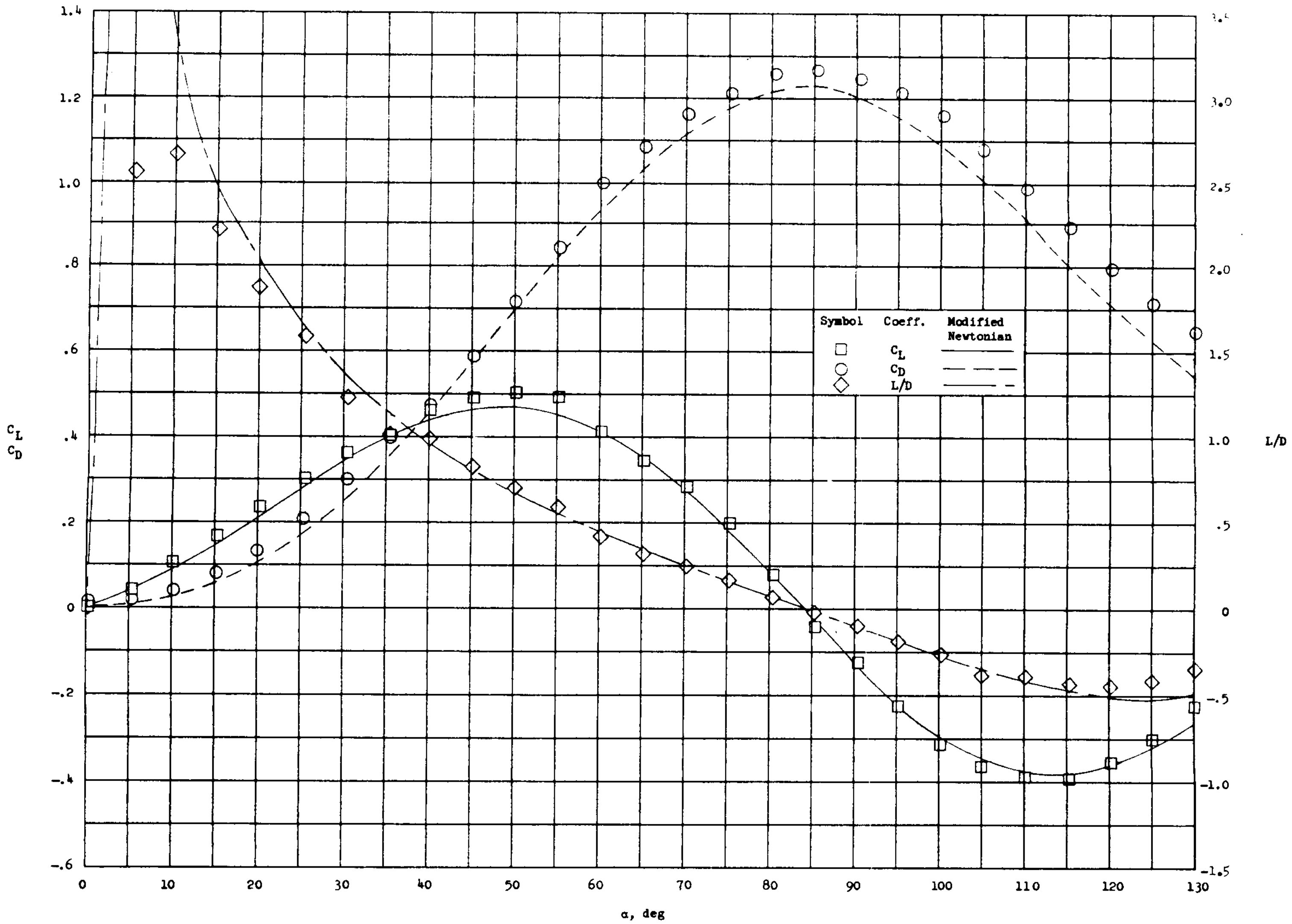

Figure 5.- Longitudinal force characteristics of cone having 5° semivertex angle. $M_\infty = 6.83$; $R_\infty = 1.25 \times 10^6$.

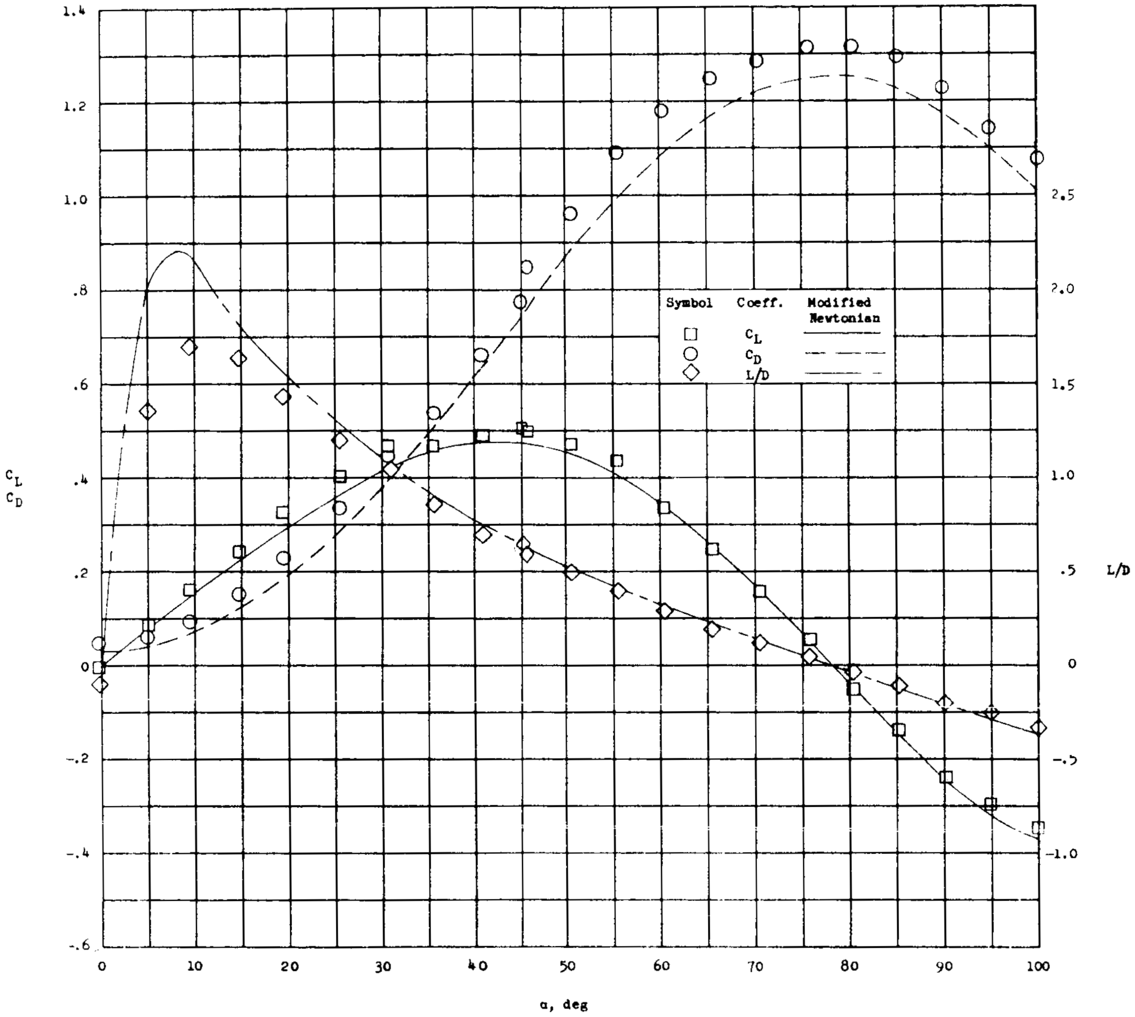

Figure 6.- Longitudinal force characteristics of cone having 10° semi-vertex angle. $M_\infty = 6.83$; $R_\infty = 0.841 \times 10^6$.

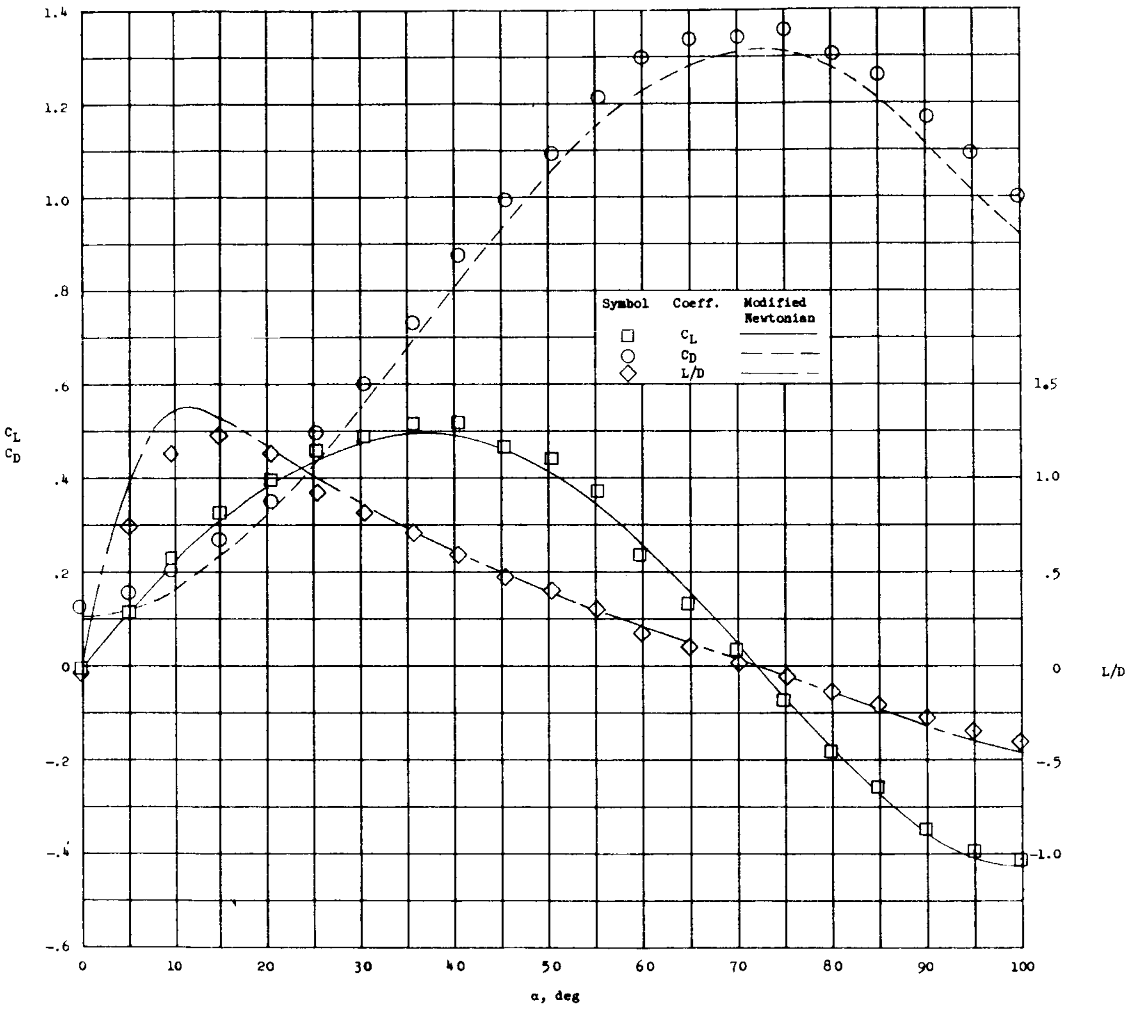

Figure 7.- Longitudinal force characteristics of cone having 15° semi-vertex angle. $M_\infty = 6.83$; $R_\infty = 0.684 \times 10^6$.

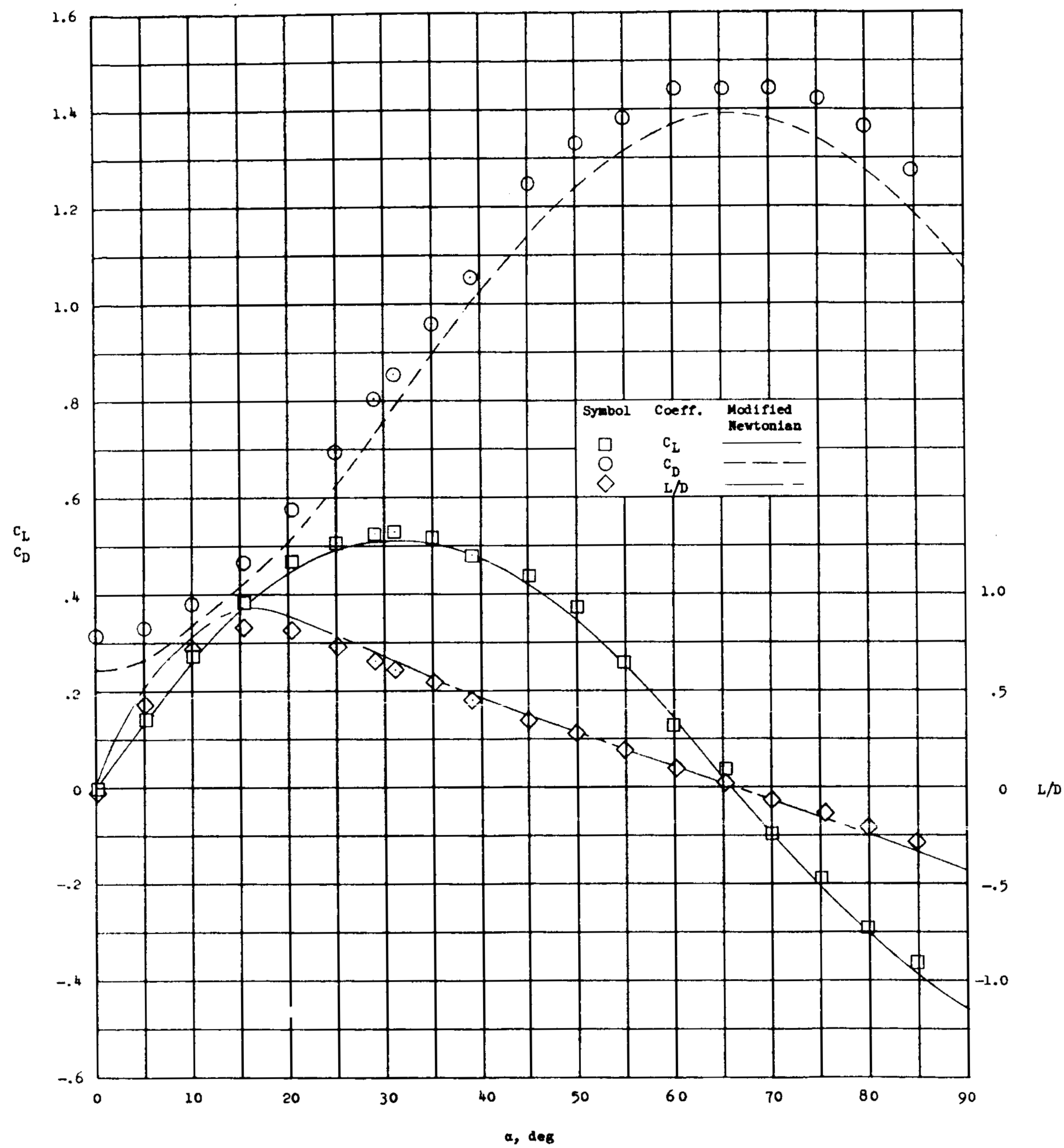

Figure 8.- Longitudinal force characteristics of cone having 20° semi-vertex angle. $M_\infty = 6.83$; $R_\infty = 0.586 \times 10^6$.

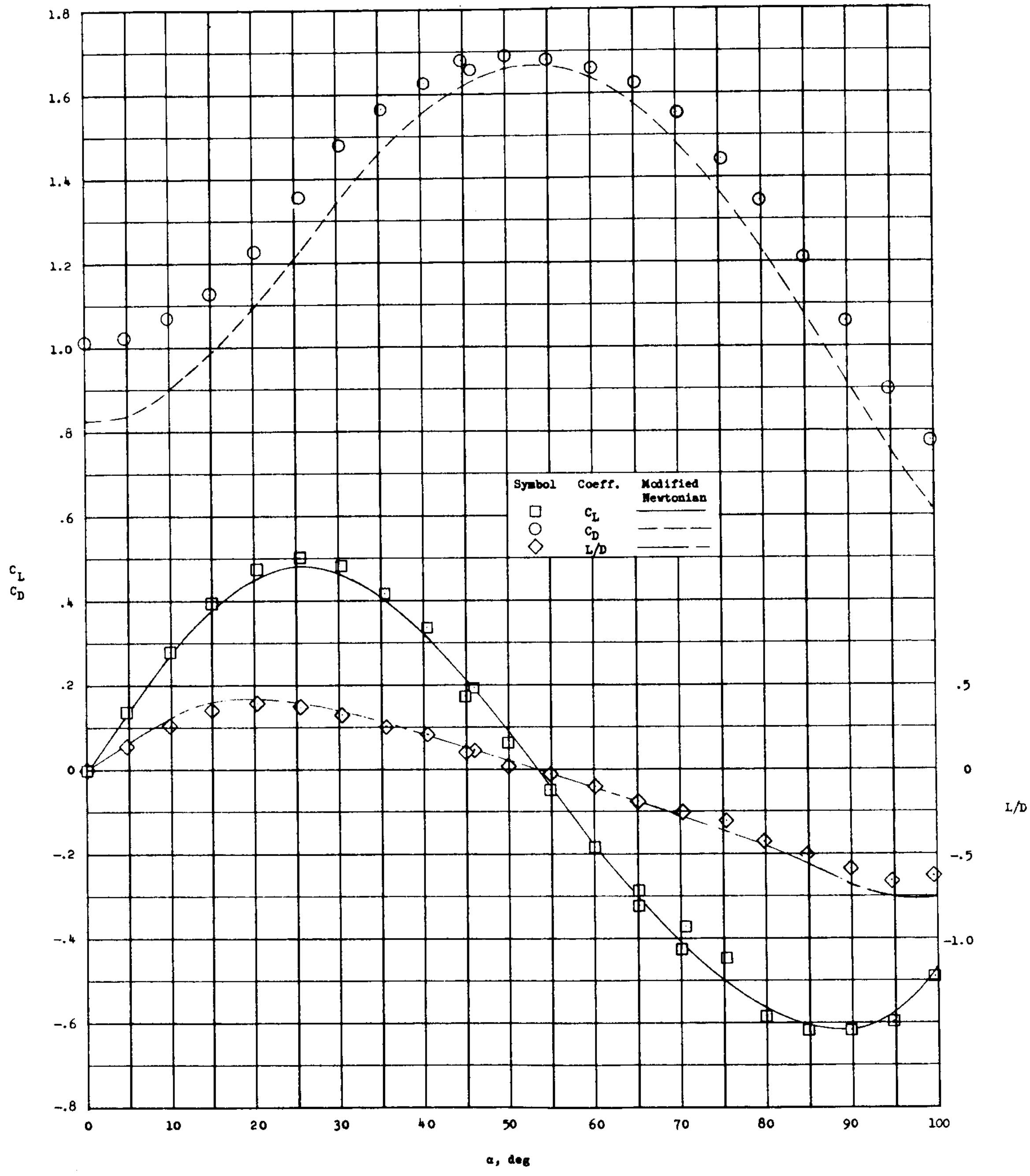

Figure 9.- Longitudinal force characteristics of cone having 30° semi-vertex angle. $M_\infty = 6.83$; $R_\infty = 0.465 \times 10^6$.

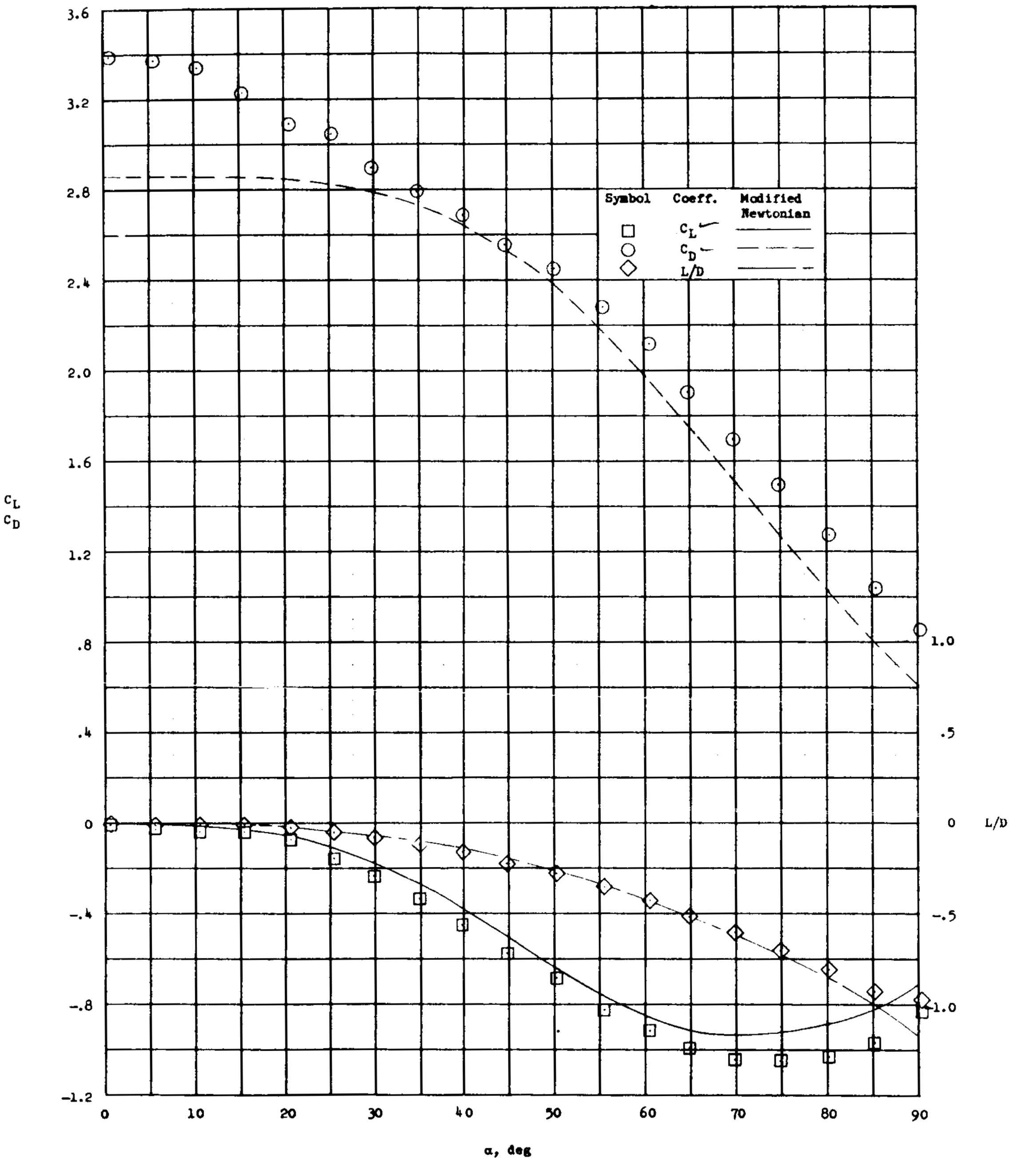

Figure 10.- Longitudinal force characteristics of cone having 45° semi-vertex angle. $M_\infty = 6.83$; $R_\infty = 0.274 \times 10^6$.

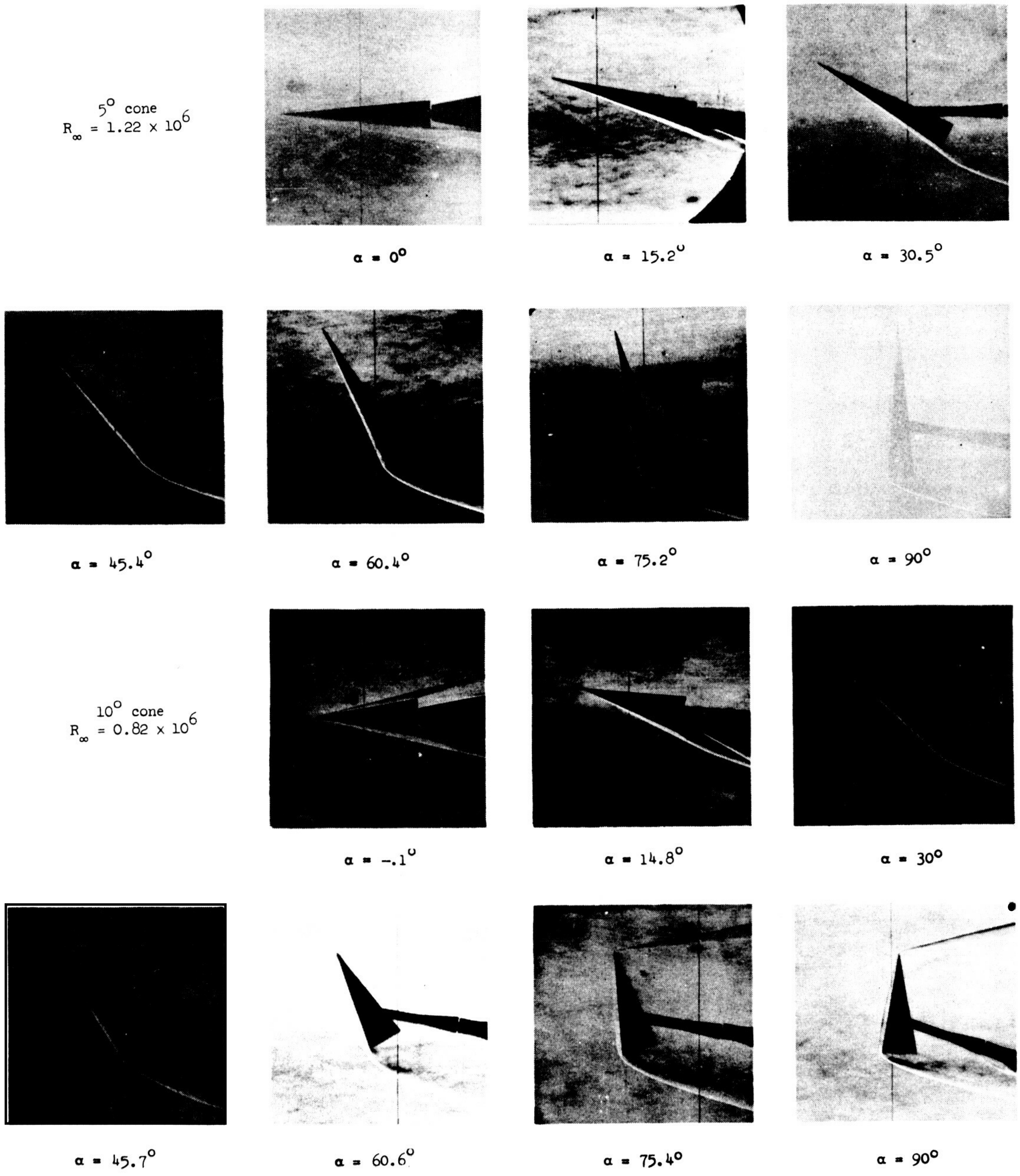

5° cone
$R_\infty = 1.22 \times 10^6$

$\alpha = 0^\circ$ $\alpha = 15.2^\circ$ $\alpha = 30.5^\circ$

$\alpha = 45.4^\circ$ $\alpha = 60.4^\circ$ $\alpha = 75.2^\circ$ $\alpha = 90^\circ$

10° cone
$R_\infty = 0.82 \times 10^6$

$\alpha = -.1^\circ$ $\alpha = 14.8^\circ$ $\alpha = 30^\circ$

$\alpha = 45.7^\circ$ $\alpha = 60.6^\circ$ $\alpha = 75.4^\circ$ $\alpha = 90^\circ$

(a) Cone models having 5° and 10° semivertex angles. L-61-1065

Figure 11.- Schlieren photographs of right-circular-cone models. $M_\infty = 6.83$.

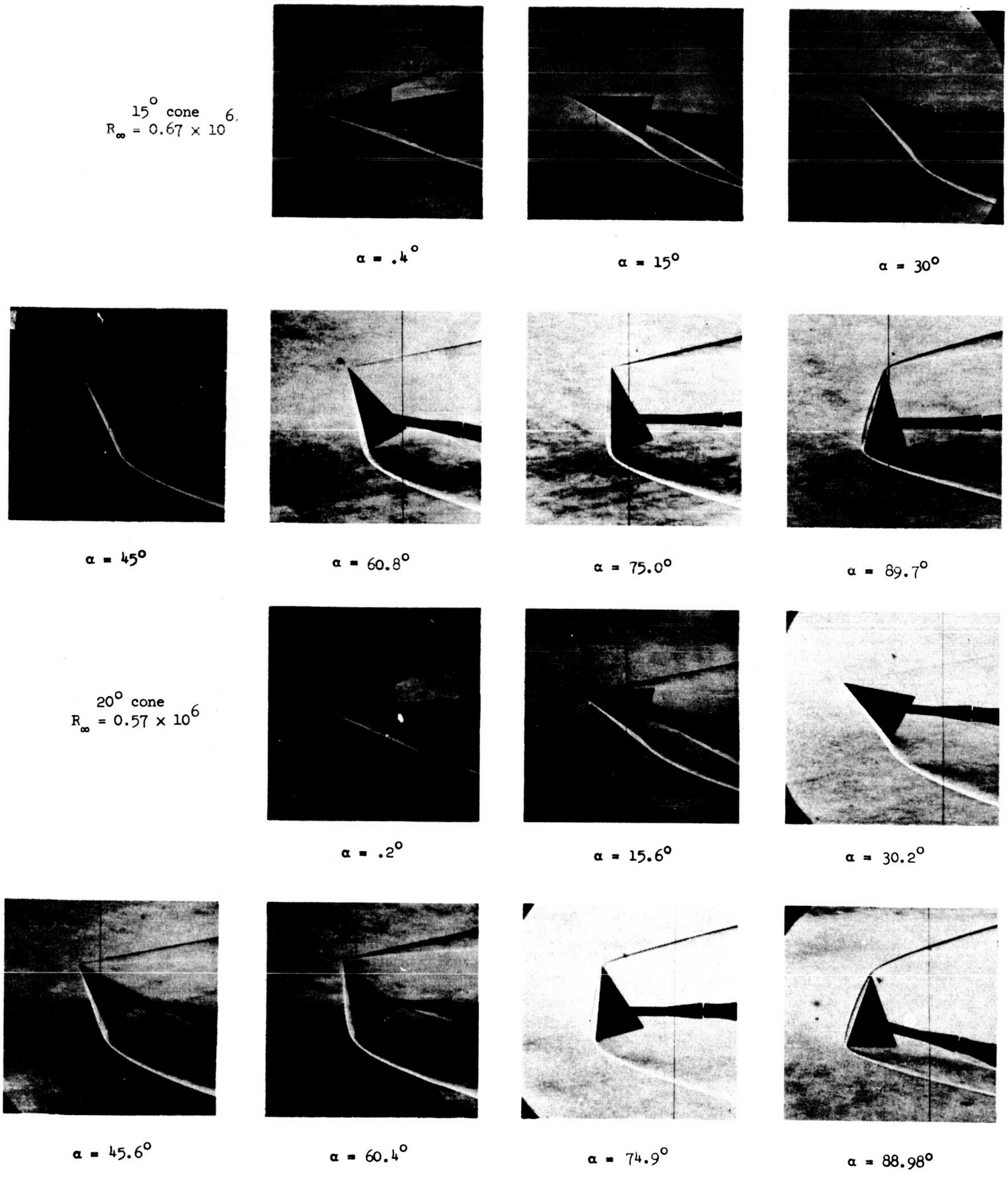

15° cone
$R_\infty = 0.67 \times 10^6$

$\alpha = .4^\circ$

$\alpha = 15^\circ$

$\alpha = 30^\circ$

$\alpha = 45^\circ$

$\alpha = 60.8^\circ$

$\alpha = 75.0^\circ$

$\alpha = 89.7^\circ$

20° cone
$R_\infty = 0.57 \times 10^6$

$\alpha = .2^\circ$

$\alpha = 15.6^\circ$

$\alpha = 30.2^\circ$

$\alpha = 45.6^\circ$

$\alpha = 60.4^\circ$

$\alpha = 74.9^\circ$

$\alpha = 88.98^\circ$

(b) Cone models having 15° and 20° semivertex angles. L-61-1066

Figure 11.- Continued.

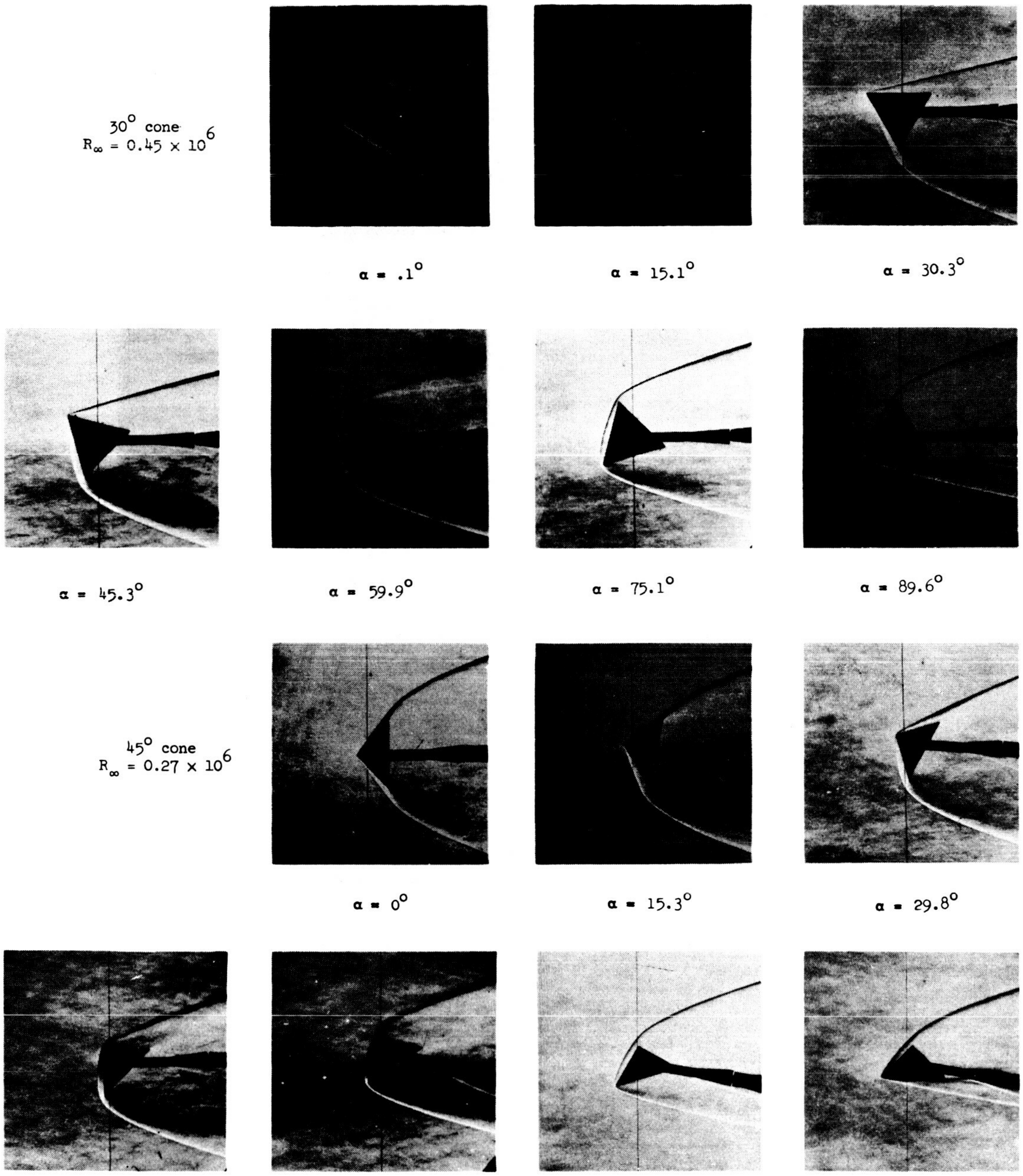

30° cone
$R_{\infty} = 0.45 \times 10^{6}$

$\alpha = .1^{\circ}$ $\alpha = 15.1^{\circ}$ $\alpha = 30.3^{\circ}$

$\alpha = 45.3^{\circ}$ $\alpha = 59.9^{\circ}$ $\alpha = 75.1^{\circ}$ $\alpha = 89.6^{\circ}$

45° cone
$R_{\infty} = 0.27 \times 10^{6}$

$\alpha = 0^{\circ}$ $\alpha = 15.3^{\circ}$ $\alpha = 29.8^{\circ}$

$\alpha = 44.5^{\circ}$ $\alpha = 60.5^{\circ}$ $\alpha = 74.9^{\circ}$ $\alpha = 90.3^{\circ}$

(c) Cone models having 30° and 45° semivertex angles. L-61-1067

Figure 11.- Concluded.

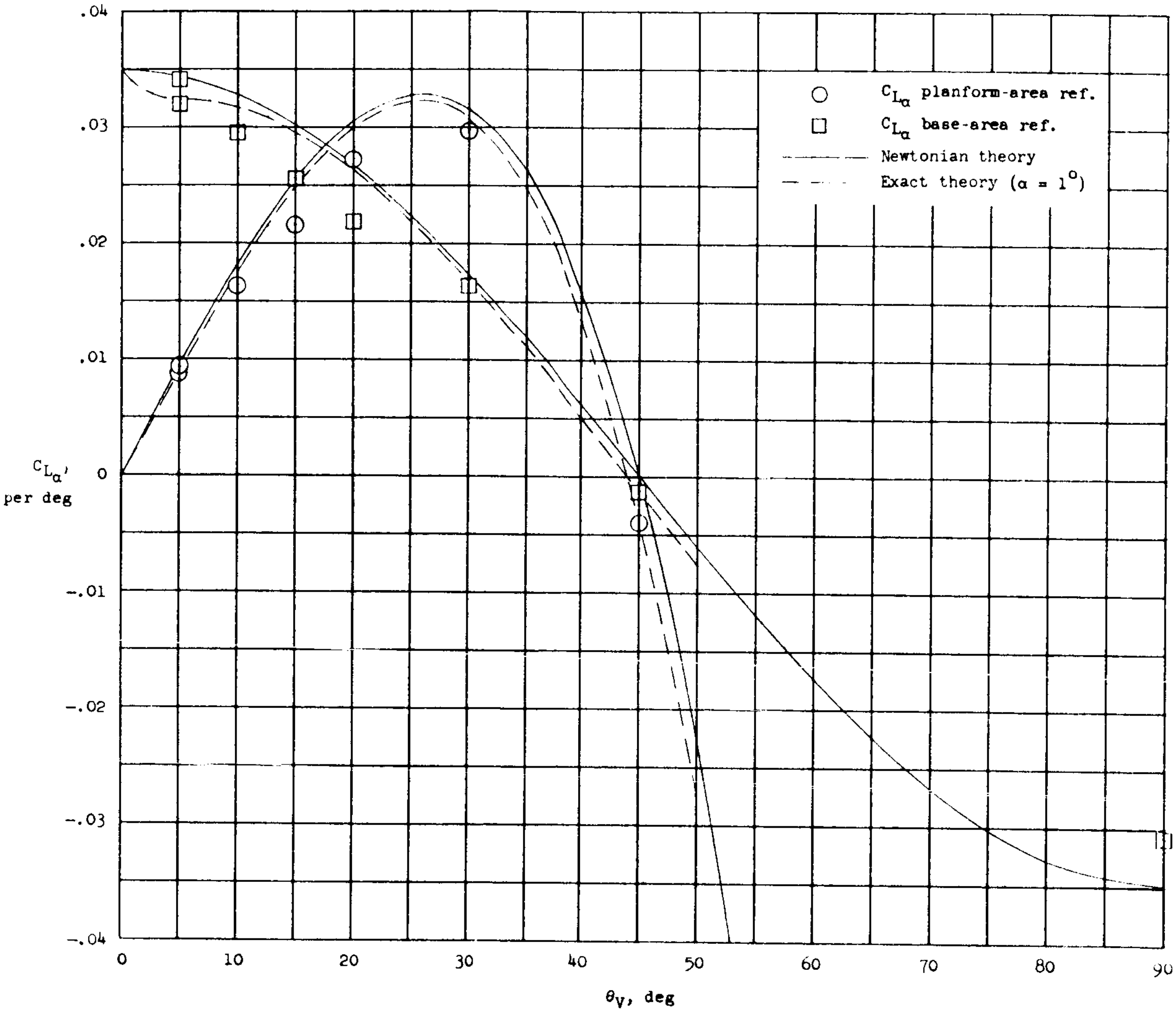

Figure 12.- Variation of lift-curve slope with cone semivertex angle for right circular cones. $M_\infty = 6.83$.

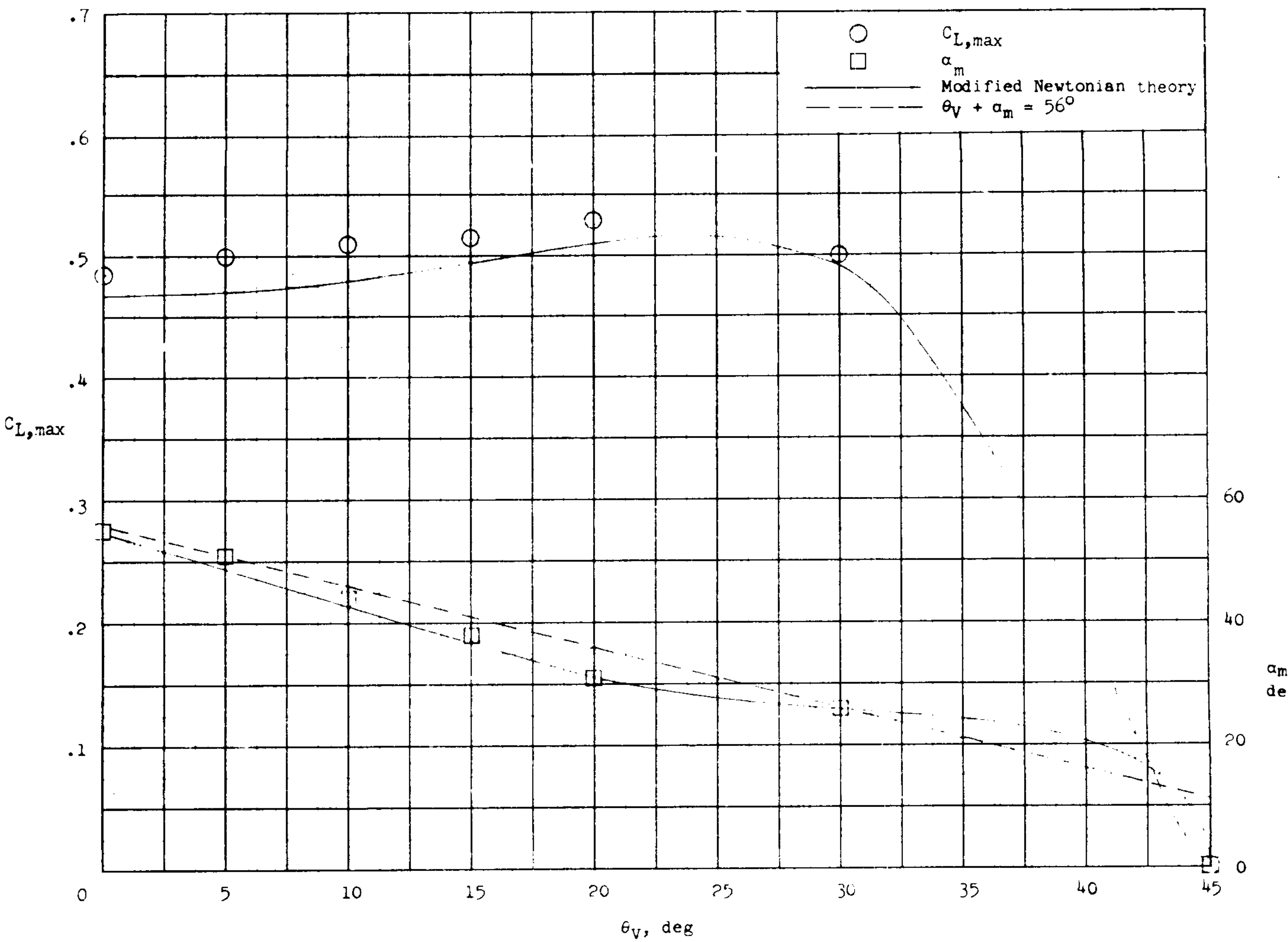

Figure 13.- Variation of maximum lift coefficient and the angle of attack at which it occurs with cone semivertex angle for right circular cones. $M_\infty = 6.83$.

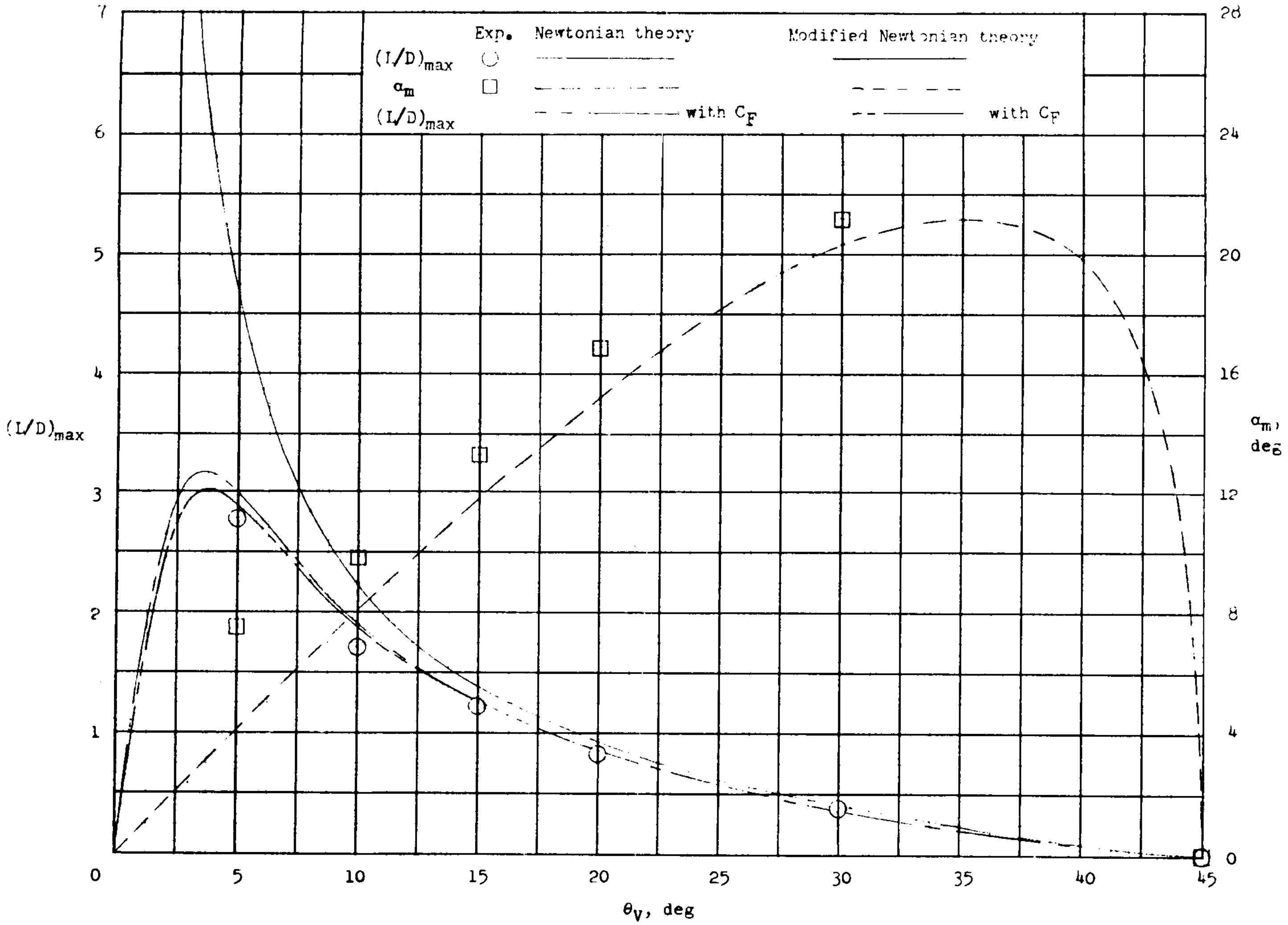

Figure 14.- Variation of maximum lift-drag ratio and the angle of attack at which it occurs with cone semivertex angle for right circular cones. $M_\infty = 6.83$.

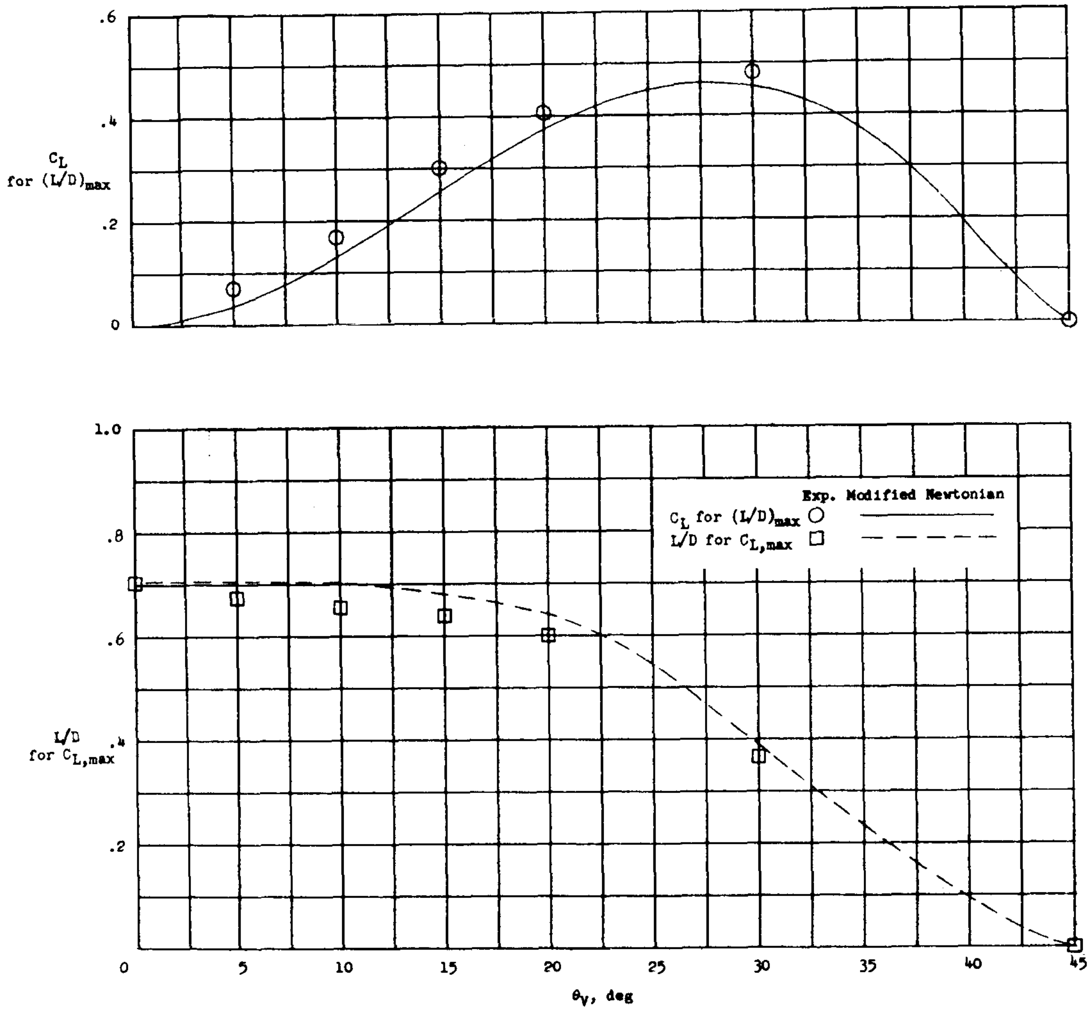

Figure 15.- Variation of lift coefficient at the point of maximum lift-drag ratio and lift-drag ratio at the point of maximum lift coefficient with cone semivertex angle for right circular cones. $M_\infty = 6.83$.

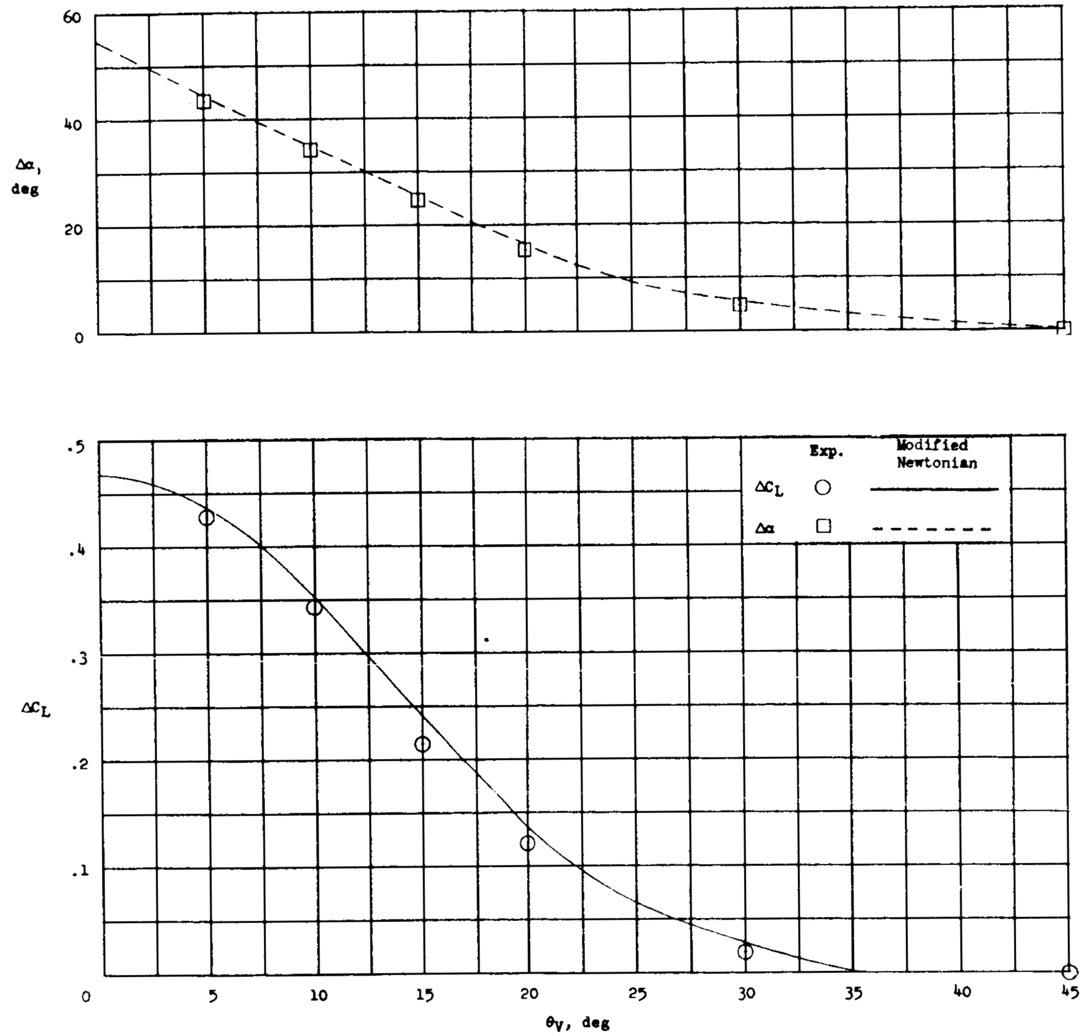

Figure 16.- Variation of the increments of angle of attack and lift coefficient between $(L/D)_{max}$ and $C_{L,max}$ with cone semivertex angle for right circular cones. $M_\infty = 6.83$.

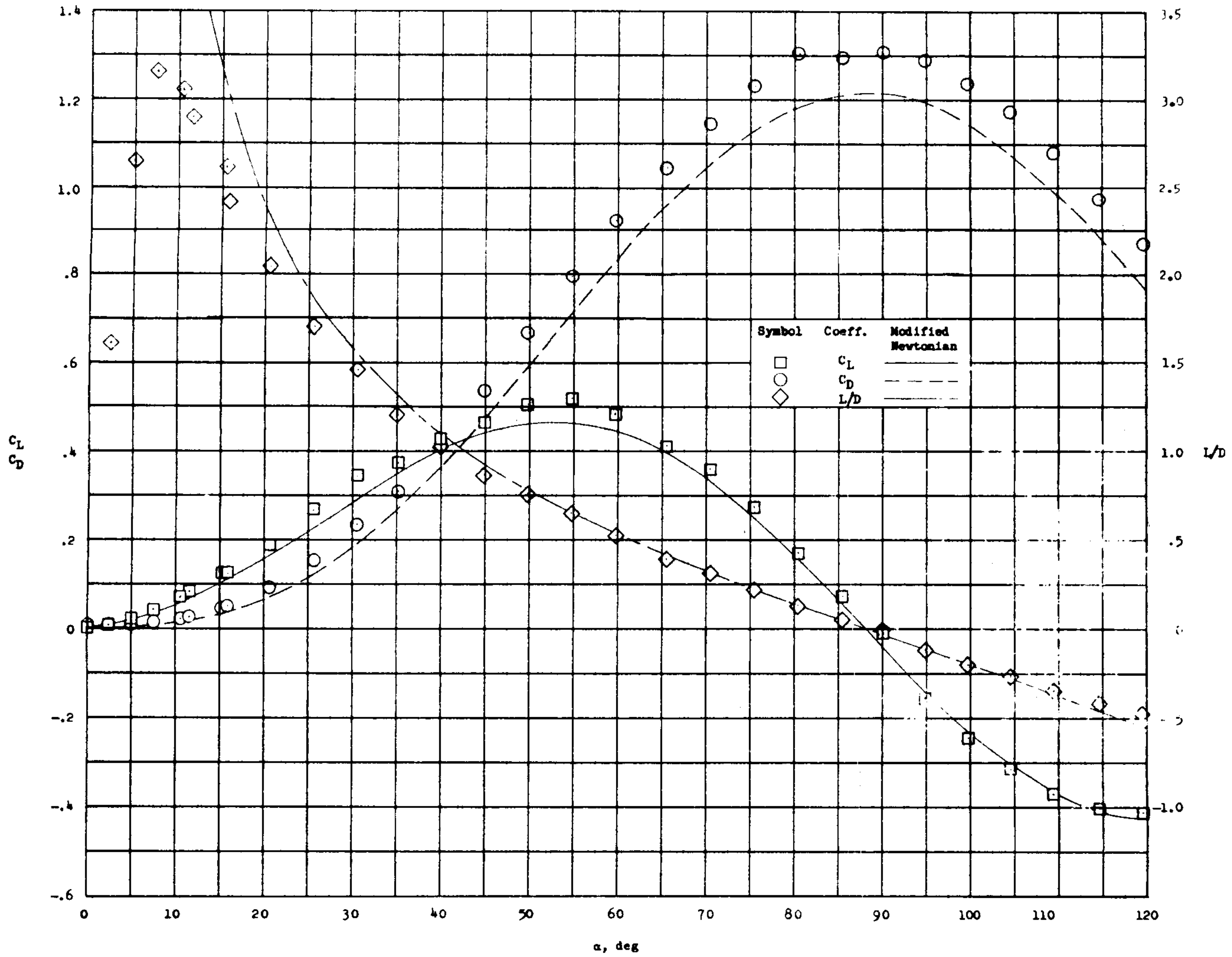

Figure 17.- Longitudinal force characteristics of a cone-cylinder configuration having a 5° semivertex angle and an afterbody fineness ratio of 6. $M_{\infty} = 6.84$; $R_{\infty} = 1.37 \times 10^{6}$.

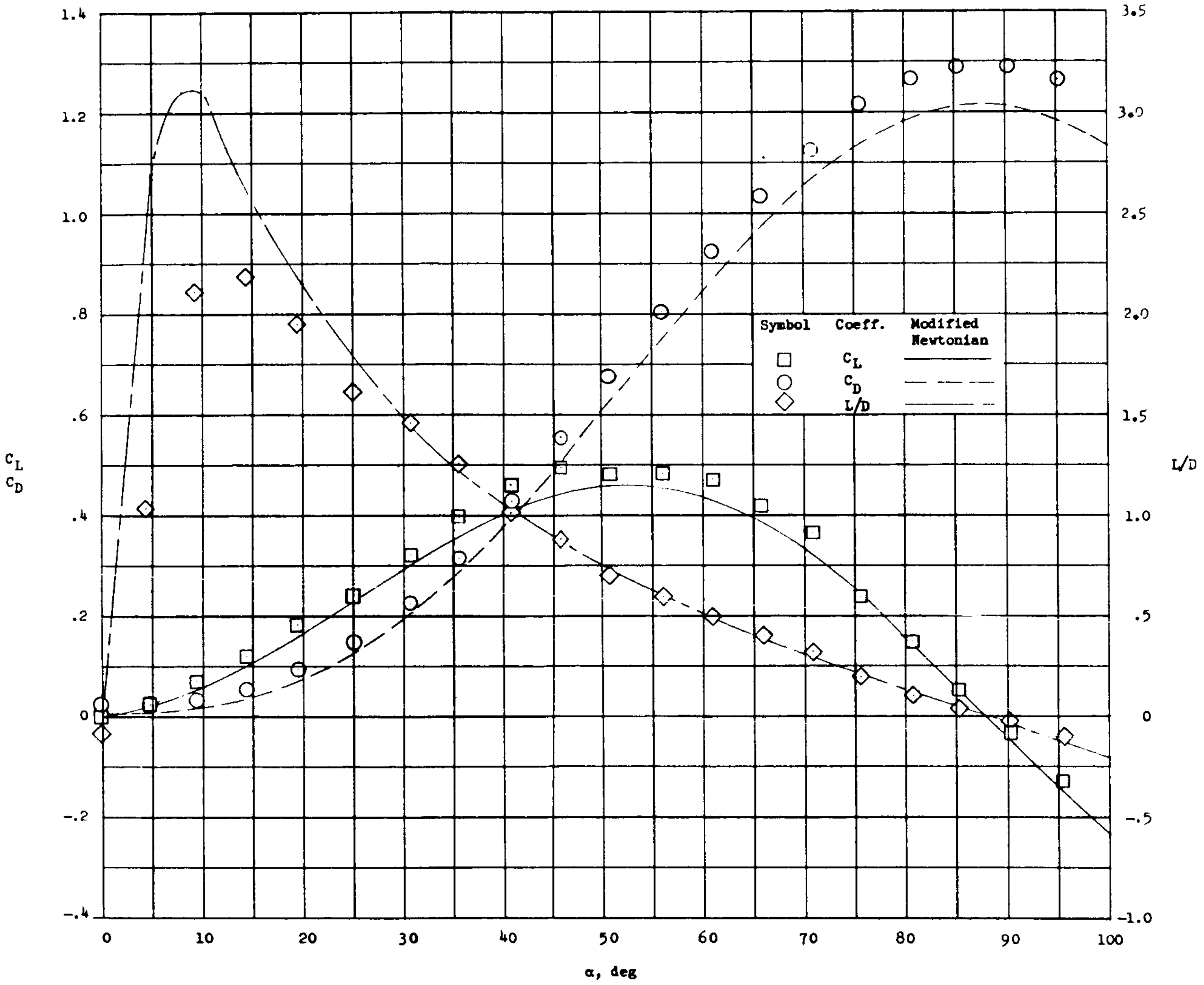

Figure 18.- Longitudinal force characteristics of a cone-cylinder configuration having a 10° semivertex angle and an afterbody fineness ratio of 6. $M_\infty = 6.83$; $R_\infty = 1.15 \times 10^6$.

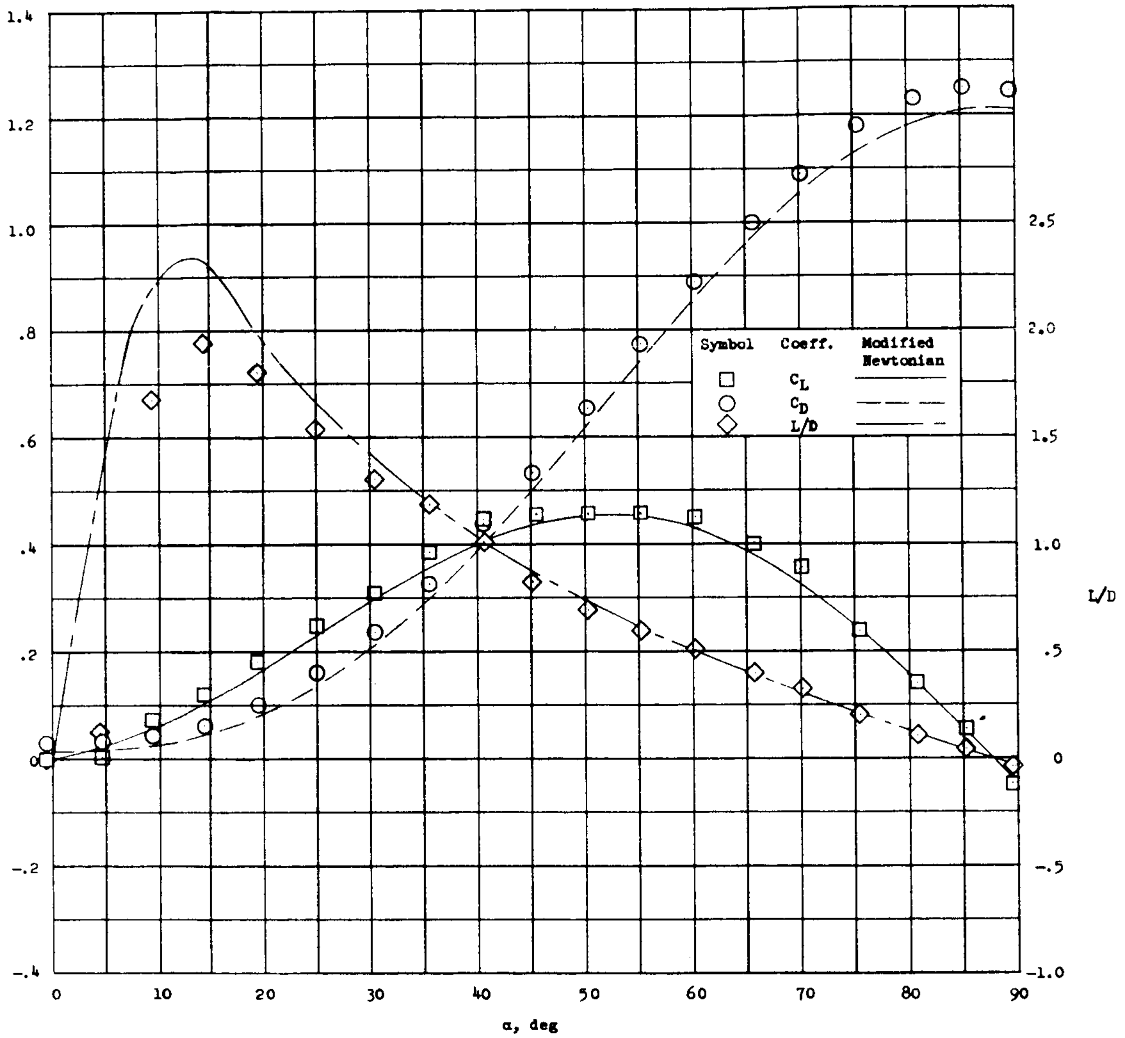

Figure 19.- Longitudinal force characteristics of a cone-cylinder configuration having a 15° semivertex angle and an afterbody fineness ratio of 6. $M_\infty = 6.83$; $R_\infty = 1.06 \times 10^6$.

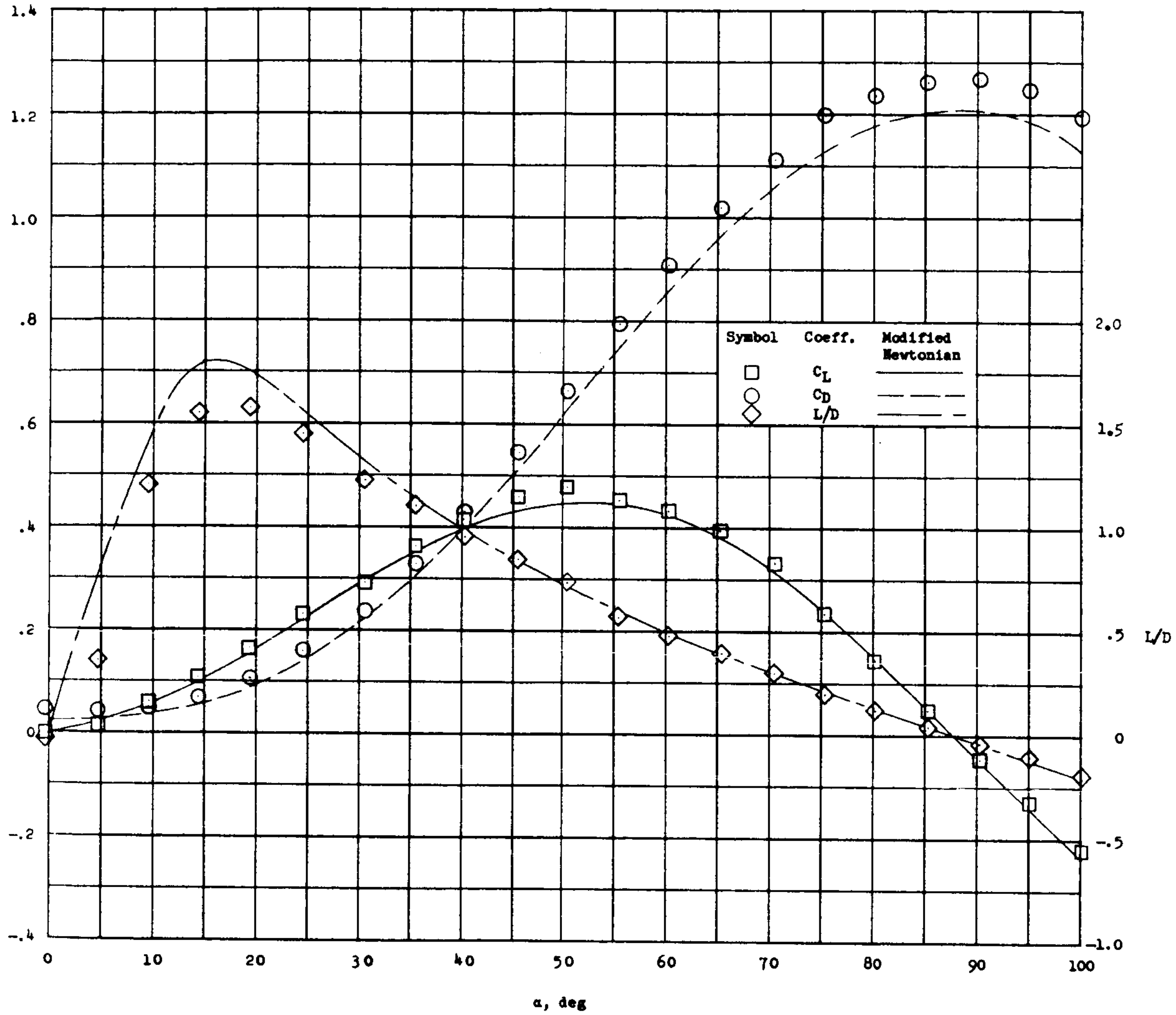

Figure 20.- Longitudinal force characteristics of a cone-cylinder configuration having a 20° semivertex angle and an afterbody fineness ratio of 6. $M_\infty = 6.83$; $R_\infty = 1.01 \times 10^6$.

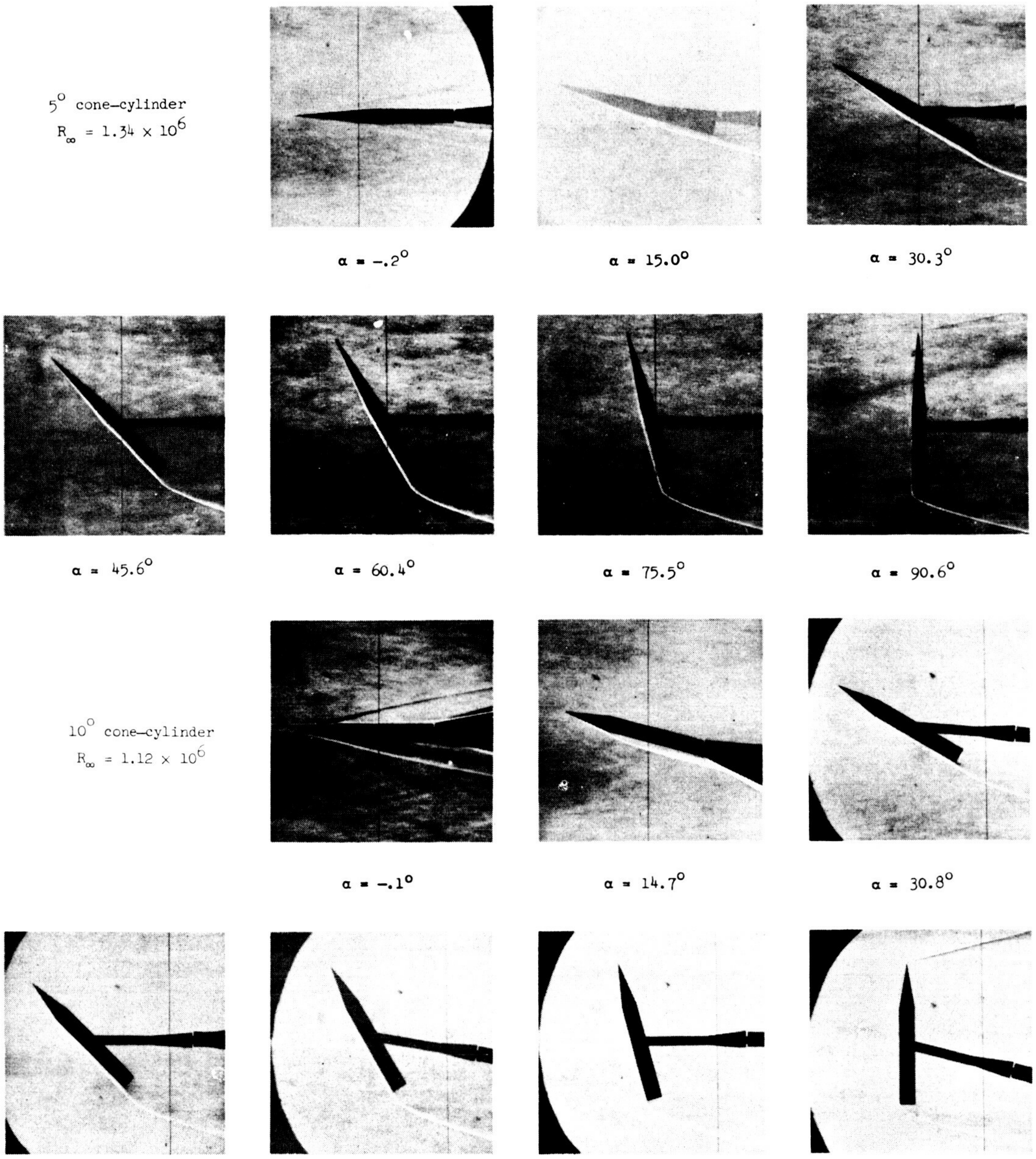
5° cone-cylinder
$R_\infty = 1.34 \times 10^6$
10° cone-cylinder
$R_\infty = 1.12 \times 10^6$

$\alpha = -.2^\circ$ $\alpha = 15.0^\circ$ $\alpha = 30.3^\circ$

$\alpha = 45.6^\circ$ $\alpha = 60.4^\circ$ $\alpha = 75.5^\circ$ $\alpha = 90.6^\circ$

$\alpha = -.1^\circ$ $\alpha = 14.7^\circ$ $\alpha = 30.8^\circ$

$\alpha = 45.3^\circ$ $\alpha = 60.9^\circ$ $\alpha = 75.6^\circ$ $\alpha = 90.3^\circ$

L-61-1068

(a) Cone-cylinder models having 5° and 10° semivertex angles.

Figure 21.- Schlieren photographs of right circular cone-cylinder models having an afterbody fineness ratio of 6. $M_\infty = 6.86$.

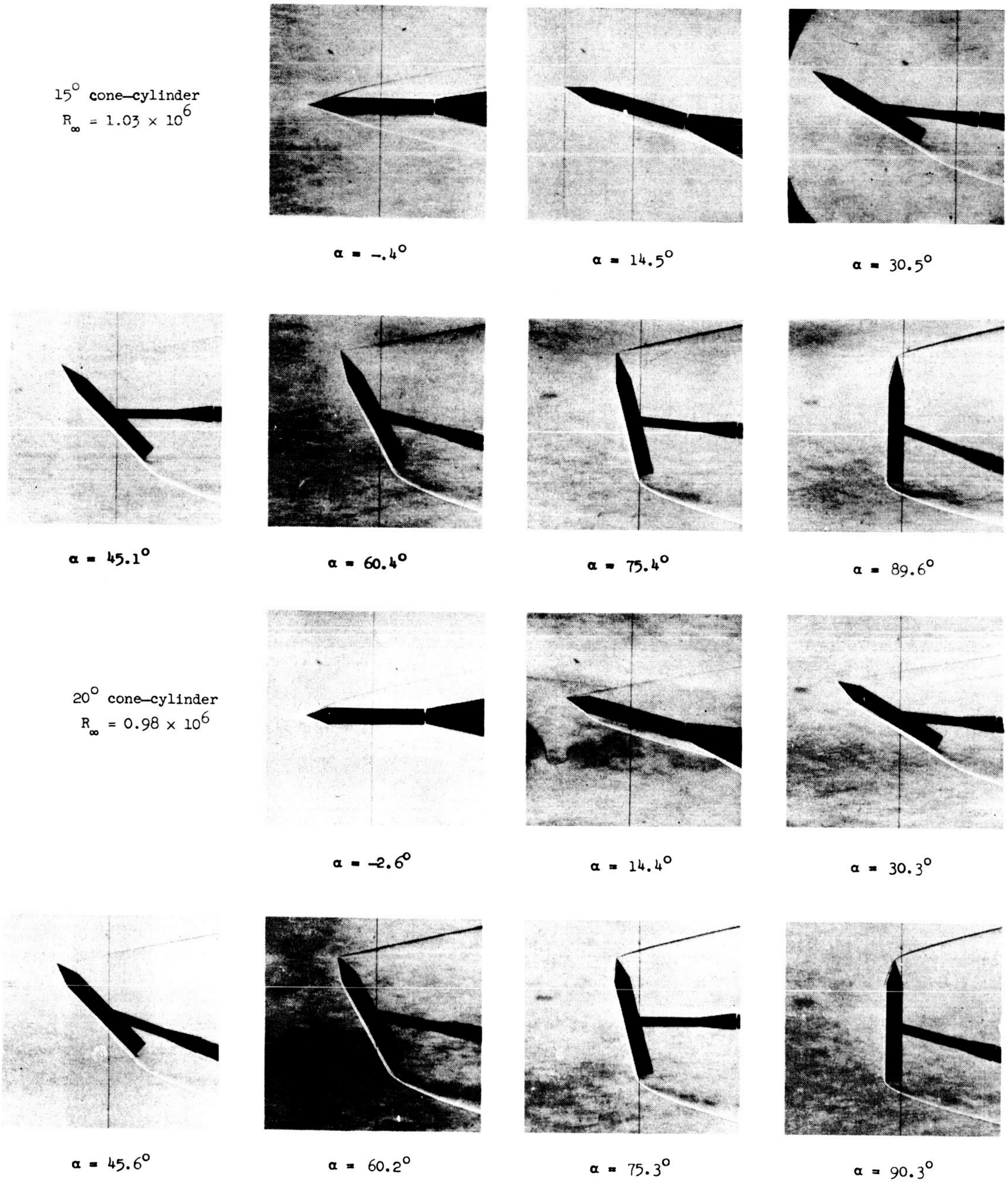

15° cone–cylinder
$R_\infty = 1.03 \times 10^6$

$\alpha = -.4^\circ$

$\alpha = 14.5^\circ$

$\alpha = 30.5^\circ$

$\alpha = 45.1^\circ$

$\alpha = 60.4^\circ$

$\alpha = 75.4^\circ$

$\alpha = 89.6^\circ$

20° cone–cylinder
$R_\infty = 0.98 \times 10^6$

$\alpha = -2.6^\circ$

$\alpha = 14.4^\circ$

$\alpha = 30.3^\circ$

$\alpha = 45.6^\circ$

$\alpha = 60.2^\circ$

$\alpha = 75.3^\circ$

$\alpha = 90.3^\circ$

L-61-1069

(b) Cone-cylinder models having 15° and 20° semivertex angles.

Figure 21.- Concluded.

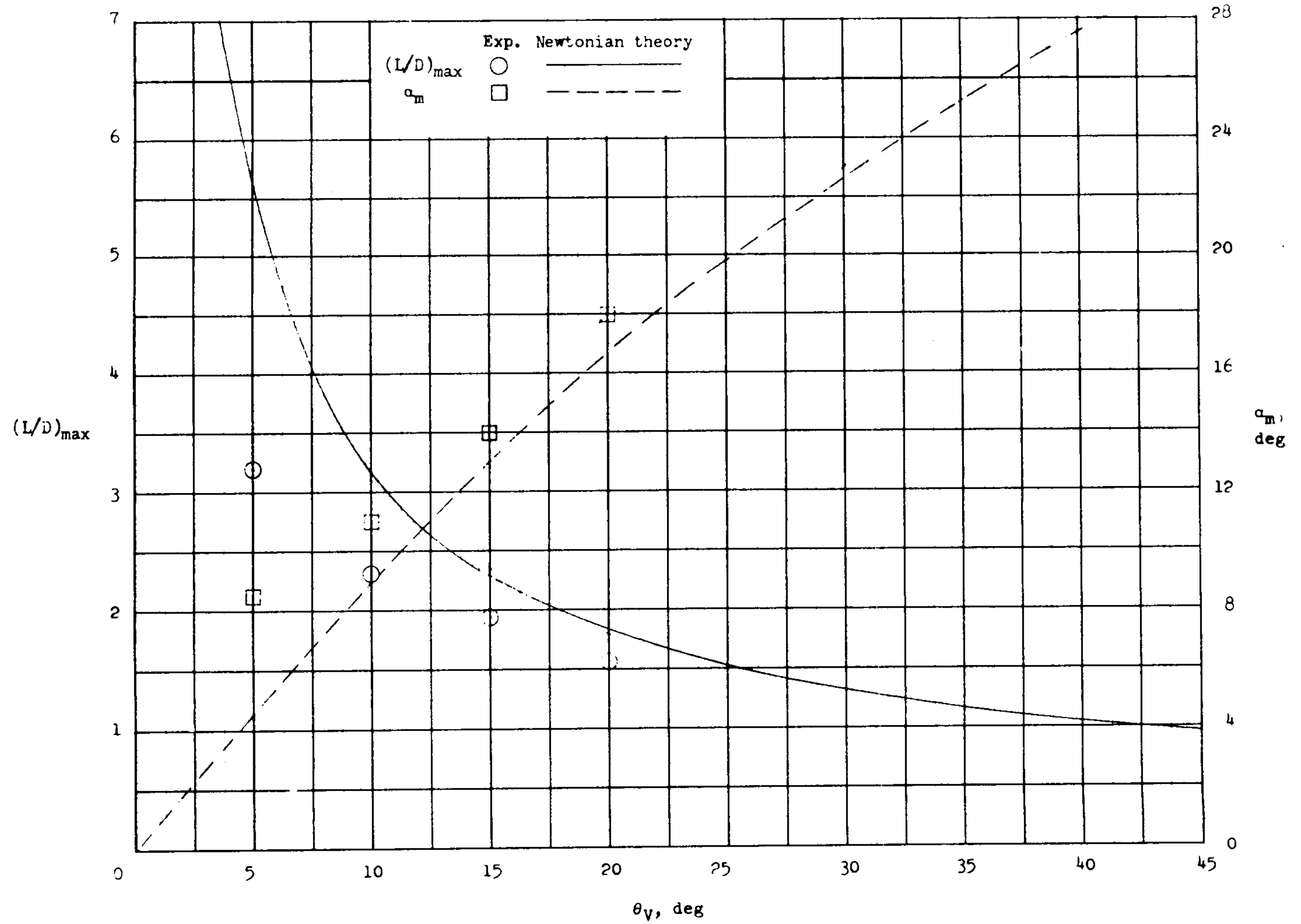

Figure 22.- Variation of maximum lift-drag ratio and the angle of attack at which it occurs with cone semivertex angle for cone-cylinder configurations having an afterbody fineness ratio of 6. $M_\infty = 6.83$.

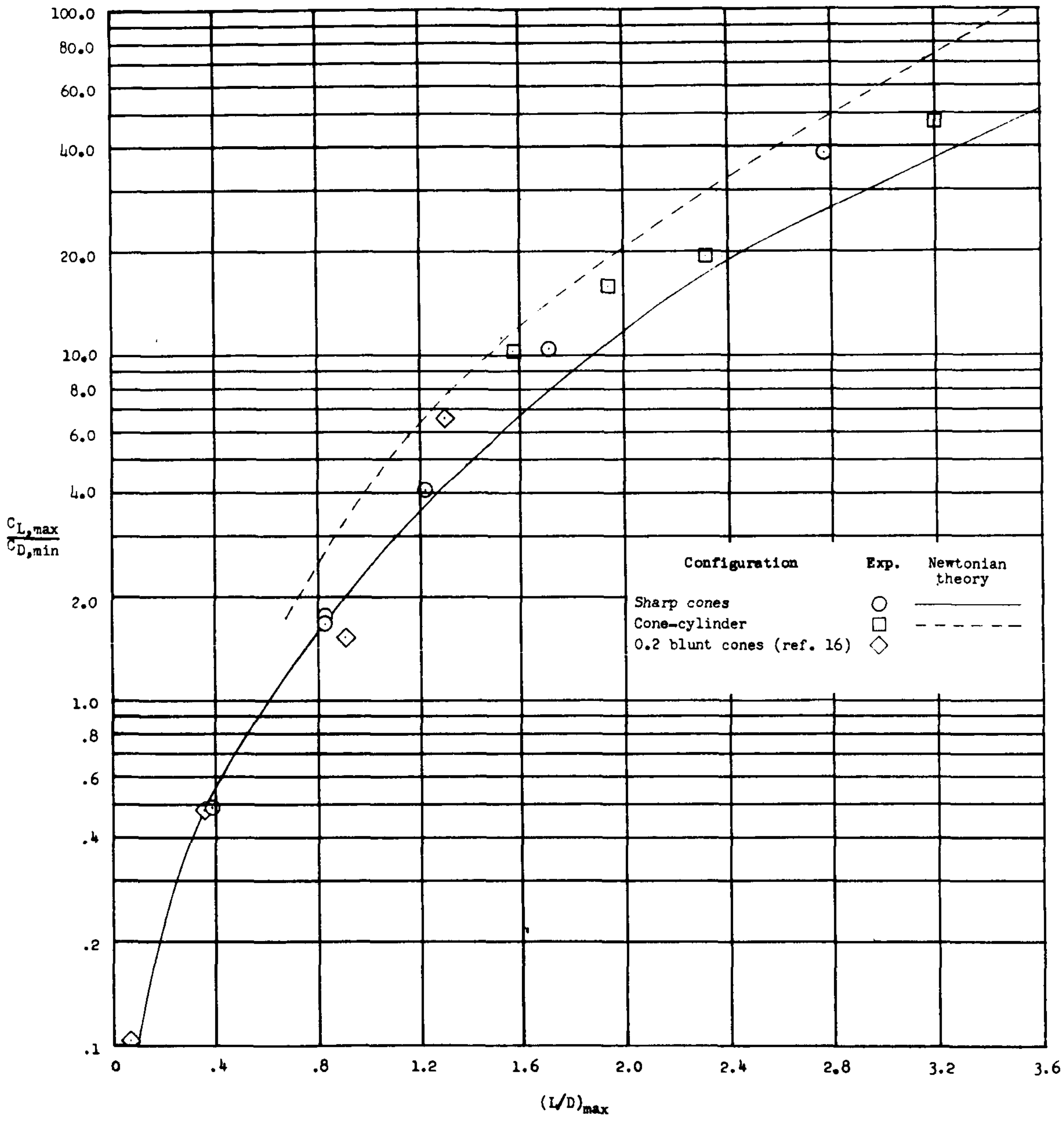

Figure 23.- Correlation of data of various lifting bodies by use of the longitudinal force parameters.